Original Research Article

Proteomic analysis of liver tissue reveals *Aeromonas hydrophila* infection mediated modulation of host metabolic pathways in *Labeo rohita*

Mehar Un Nissa[1], Nevil Pinto[2], Biplab Ghosh[3], Urvi Singh[4], Mukunda Goswami[2]* and Sanjeeva Srivastava[1]*

[1]Department of Biosciences and Bioengineering, Indian Institute of Technology Bombay, Powai, Mumbai 400076, India

[2]Central Institute of Fisheries Education, Indian Council of Agricultural Research, Versova, Mumbai, Maharashtra 400061

[3]Regional Centre for Biotechnology, Faridabad, 121001, India

[4]Department of Biochemistry, Sri Venkateswara College, University of Delhi, India

*Correspondence for proteomics work: Dr. Sanjeeva Srivastava, E-mail: sanjeeva@iitb.ac.in, Phone: +91-22-2576-7779, Fax: +91-22-2572-3480

*Correspondence for fish work: Dr. Mukunda Goswami, E-mail: mukugoswami@gmail.com

ABSTRACT

Aeromonas hydrophila (Ah) is an opportunistic Gram-negative bacterium and a serious global pathogen causing Motile Aeromonas Septicaemia (MAS) in fish and many other vertebrates. The pathogenesis of aeromonas septicaemia is complex and involves multiple perturbed pathways. Molecular analysis of host tissues could be a powerful approach to identify mechanistic and diagnostic immune signatures of disease. We performed a deep proteomic analysis of *Labeo rohita* liver tissue to examine changes in the host proteome during *Ah* infection. A total of 2525 proteins were identified of which 158 were found differentially expressed during *Ah* infection. Functional analysis of significant proteins identified the dysregulation of several metabolic enzymes, antioxidative proteins, cytoskeletal proteins and immune related proteins. Proteomic analysis revealed the alterations in the cellular defence mechanisms including phagolysosomal killing and apoptosis during *Ah* infection. Our systemic approach revealed the protein dynamics in the host cells to explore the putative biological processes underlying the metabolic reprogramming of the host cells during *Ah* infection. Our findings paved the way for future research into the role of Toll-like receptors (Tlr3), C-type lectins (Clec4e) and metabolic enzymes in *Ah* pathogenesis leading towards host directed immunotherapies to tackle the *Ah* infection in fish.

IMPORTANCE

Bacterial disease is one of the most serious problems in aquaculture industry. *Aeromonas hydrophila* (*Ah*), a Gram-negative bacterium causes motile aeromonas septicaemia (MAS) in fish. Small molecules that target the metabolism of the host have recently emerged as potential treatment possibilities in infectious diseases. However, the ability to develop new therapies is hampered due to lack of knowledge about pathogenesis mechanisms and host-pathogen interactions. Molecular level analysis of host tissues could be helpful in finding mechanistic immunological markers of diseases. We examined alterations in the host proteome during *Ah*

infection in *Labeo rohita* liver tissue to find cellular proteins and processes affected by *Ah* infection. Our systemic approach revealed protein dynamics underlying the host cells' metabolic reprogramming during *Ah* infection. Our work is an important step towards leveraging host metabolism in targeting the disease by providing a bigger picture on proteome pathology correlation during *Ah* infection.

Keywords: *Aeromonas hydrophila*, Liver proteomics, reprogramming, mass spectrometry, rohu

Abbreviations:

Aars	Alanine--tRNA ligase OS
Atp2b1	Calcium-transporting ATPase
Atp6v1a	H(+)-transporting two-sector ATPase
Atp6voc	V-type proton ATPase proteolipid subunit
Atp8	ATP synthase protein 8 OS
Cpt1	Carnitine O-palmitoyltransferase OS
Cyp1a	Unspecific monooxygenase OS
Cyp2f2	Cytochrome P450 2F2-like protein OS
Cyp2g1	Cytochrome P450 2G1-like protein
Cyp3a	Cytochrome P450 3A30-like protein OS
Eprs	Glutamyl-tRNA synthetase OS
Fabp	Fatty acid-binding brain-like protein OS
Hsp90aa1	Heat shock HSP 90-alpha OS
Hspa8	Heat shock cognate 71 kDa OS
Mogs	Mannosyl-oligosaccharide glucosidase-like protein OS
Ndufa12	NADH dehydrogenase [ubiquinone] 1 alpha subcomplex subunit 12
Ndufa2	Complex I-B8 OS
Ndufa6	Complex I-B14
Ndufb10	Complex I-PDSW OS
Ndufb6	Complex I-B17
Ndufs8	Complex I-23kD
Ndufv2	NADH dehydrogenase [ubiquinone] flavoprotein 2, mitochondrial
Psma1	Proteasome subunit alpha type-1
Psma5	Proteasome subunit alpha type OS
Psma8	Proteasome subunit alpha type OS
Psmb4	Proteasome subunit beta
Psmd3	26S proteasome non-ATPase regulatory subunit 3 OS
Psmd6	26S proteasome non-ATPase regulatory subunit 6 OS
Qars	Glutamine--tRNA ligase OS
Rpl13	60S ribosomal protein L13 OS
Rpl7a	60S ribosomal protein L7a OS

Rplp2	60S acidic ribosomal protein P2 OS
Rps6	40S ribosomal protein S6 OS
Rrbp1	Ribosome-binding 1-like isoform X1 OS
Scp2	Acetyl-CoA C-myristoyltransferase OS
Sec31a	Transport Sec31A-like isoform X5 OS
TCEP	Tris(2-carboxyethyl)phosphine
Tlr4	Toll-like receptor 4

INTRODUCTION

The intensification of aquaculture system leads to the occurrence of diseases that reduce the quality of fish and fishery products and in turn cause economic loss. Aquaculture is experiencing a massive loss of production due to a variety of reasons of which more than 50% are due to diseases especially in developing countries (1). Aeromonads have been recognised as the most common bacterial pathogens responsible for bacterial fish diseases. Aeromonads include *Aeromonas hydrophila (Ah), A. veronii, A. sobria,* and *A. caviae* which harm a wide range of hosts (2). Among these, *Ah* is highly infective and results in economic loss at alarming levels (3). *Ah* is a gram-negative opportunistic pathogen. Infectious signs of dropsy, hemorrhages, ulcers and necrosis have been observed in all stages of carps and other freshwater fish species like *Arapaima gigas*, Nile tilapia (*Oreochromis niloticus*) and catfish (4–7).

Proteomic analysis has become crucial for understanding the fundamental mechanisms of bacterial resistance and virulence. This has resulted in a greater understanding of pathogen biology and interaction with host that can be well addressed through holistic approaches like proteomics (8). Proteomics approaches have been utilised to explore the antibiotic resistance mechanism in *Ah.* With the help of proteomic approaches, it has been reported that the quinolones resistance in *Ah* might involve increased expression of SOS response-related proteins while decreasing those of chemotaxis (9). Further, the proteomic analysis of carp intestinal mucosa revealed that the differentially expressed proteins belong to MHC II protein complex and immune response, throwing light on the metabolic processes that are important during *Ah* infection (10). In *Ah* infected Wuchang bream (*Megalobrama amblycephala*), proteomic analysis of hepatopancreas revealed that *Ah* infection affected antioxidative proteins through complex regulatory mechanisms and decreased immunological ability (11). In the gills of Zebrafish, mucosal immune response was found enhanced during *Ah* infection (12).

Fish majorly depend on their innate immune system as their first line of defense which is an important factor in disease resistance (13). *Ah* infections cause changes in the host metabolism, but the mechanisms that determine the nature and severity of these changes are still not known completely. In order to explore the infection mediated metabolic changes in the host, we performed proteomic analysis of liver tissue of *Ah* infected *Labeo rohita. L. rohita* is the most important aquaculture species among the three Indian major carp species in polyculture system. Liver is a metabolically active tissue and has been recognized as a central immunological organ with high exposure to circulating antigens and endotoxins from the gut microbiota, particularly enriched for innate immune cells (14). This study focussed on proteomic characterisation of infected liver to understand *Ah* pathogenesis and to look into the physiological changes and host response to *Ah* infection.

RESULTS

Aeromonas hydrophila infection alters proteomic profile in host liver tissue

Discovery based proteomics data was acquired for eight samples (Details in Material and Methods) through high resolution mass spectrometry and a label-free quantitation (LFQ) approach was utilised for detection and quantification of the host proteins. The significantly altered proteins (p-value 0.05) were considered for the identification of the best panel of proteins to differentiate the control and *Ah* infected group. Further using a targeted mass spectrometry-based approach of selected/multiple reaction monitoring (SRM/MRM), selected protein targets were validated where data was acquired for eleven samples (five AH and six Control). Finally, we looked into how *Ah* (Ah) infection impacted the host's physiological processes (Fig. 1).

Comparison of proteomic profiles from uninfected and infected liver tissue was performed to define changes to the host proteome during *Ah* infection. After analysing through label-free quantification approach, on an average ~1650 proteins were quantified in each replicate (Table S1) except one of the samples from infected group (AH1) which was removed from downstream analysis because of poor mass spectrometric results compared to other samples (Fig. S1A-B). Further statistical analysis was performed for 7 out of 8 samples; four of the control samples (Liv-C1 to Liv-C4) and three infected samples (Liv-AH2 to Liv-AH4). We observed 390 proteins to be enriched in control group (viz. quantified in at least 75% of control samples and not detected or detected in less than 33% samples of AH condition) and concurrently 113 proteins were enriched in AH group (*Ah* infected) which might be a reflection of different proteome expression under healthy and diseased condition (Fig. S1C, Table S1). Differential expression analysis was performed for 1157 overlapped proteins between the two groups. In comparison to the control group, we observed that in the *Ah* infected group, 59 proteins exhibited a decreased abundance while 98 proteins showed an increased abundance

representing a total of 157 dysregulated proteins during *Ah* infection (Fig. 2A, Table S1) (see Materials and Methods for significance threshold values). We employed Partial Least Squares Discriminant Analysis (PLS-DA) to identify the proteins that can distinguish the AH group (*Ah* infected) from the Control group on the basis of variable importance in projection (VIP) Score. Top 30 features (proteins) that can clearly classify between two groups are represented (Fig. 2B). Unsupervised hierarchical clustering analysis clearly clustered the samples with similar abundance profiles and stratified the bacterial infected and control group as represented for top 30 features (Fig. 2C). Proteins that could differentiate the infected group form control group mapped to diverse molecular functions as described below. Comparative protein abundances for few of the differentially expressed proteins is represented in Fig. 2D including Metalloreductase STEAP4 (Steap4), Glutamine gamma-glutamyltransferase (Tgm1) and Actin-related protein 2 (Actr2) showing increased abundance and Biotinidase (Btd), Toll-like receptor 3 (Tlr3), Antithrombin-III-like isoform X1 (Serpinc1) proteins showing a decreased abundance as a result of *Ah* infection.

Differentially expressed proteins (DEPs) along with the proteins quantified only in one group (i.e., Control enriched or AH enriched) were considered for functional analysis (gene ontology) to further look into their biological association. Proteins that showed decreased abundance in AH group (*Ah* infected) belong to the processes like metabolism of amino acids, endopeptidase and peptidase activity, lysosomal processes, oxidoreductase activity and innate immune system. However, proteins with increased abundance during the infection were mainly mapped to carboxylic acid metabolism, cellular amide metabolism, Cytoplasmic ribosomal components, cytoplasmic translation and ligase activity (Fig. 2E, Fig. S2, Table S2).

Dynamics of host metabolic pathways and protein-protein interactions during Ah infection

We performed protein-protein interaction (PPI) and pathway analysis for the DEPs and enriched proteins to see how the *Ah* infection affected the overall composition of the liver

proteome. For the downregulated proteins, the enriched pathways and processes include the processes like lysosome, apoptosis, metabolism of xenobiotics by cytochrome P450, retinol metabolism, pantothenate metabolism, beta alanine metabolism, drug metabolism, metabolism of RNA and endocytosis (Fig. 3A-B). Pathway enrichment analysis of the upregulated proteins revealed the involvement of these proteins in several biological processes and pathways including innate immune system, signaling of B cell receptor, proteosome pathway, ribosome, carbon metabolism, protein synthesis (translation) and protein processing in ER (Fig. 3C-D). Dysregulation of these processes may indicate the severity of infection and its adverse effects on overall physiological processes.

A. hydrophila infection alters anti-oxidative defence system and hepatic xenobiotic metabolism

Infections are generally accompanied by a disturbance of the normal cellular homeostasis. Biotinidase protein (Btd) expression was found to be decreased by 7-folds during *Ah* infection (Fig. 2D, Table S1). Biotinidase recycles protein-bound biotin, resulting in the regeneration of free biotin which is essential for carbohydrate, protein and fat metabolism. Biotin deficiency has been reported to impair normal growth and immune functions (15). Another protein Antithrombin-III-like isoform X1 (Serpinc1) was also decreased by ~7 folds during *Ah* infection. Antithrombin is a natural coagulant synthesised in the liver and also involved in the anti-inflammatory signaling responses (16). Proteins like Glutathione transferase (Gst-A0A498NKS6), Glutathione peroxidase, Cytochrome P450 family (Cyp1a, Cyp2f2), Epoxide hydrolase (Ephx1), Dihydropyrimidinase (Dpys) and Dihydropyrimidine dehydrogenase [NADP (+)] (Dypd), involved in Xenobiotics and Drug metabolism (17) were downregulated during *Ah* infection. Proteins related to antioxidative system were also downregulated such as Peroxiredoxin-4 (Prdx4), Gst and Prenylcysteine oxidase 1 (Pcyox1). Downregulated proteins were also mapped to biological processes involved in general functions of liver such as

Monooxygenase (Cypa1a) and Epidermal retinol dehydrogenase 2-like protein (Sdr16C5) from Retinol metabolism, Dihydropyrimidinase (dpys) and Dihydropyrimidine dehydrogenase (dpydb) from Pantothenate and CoA biosynthesis and beta-Alanine metabolism, Glycine hydroxymethyltransferase (Shmt2) which is involved in several biological processes like carboxylic acid metabolism, amino acid metabolim and energy metabolic processes (Fig. 3A, Table S2).

A. hydrophila infection alters the cytoskeleton, lysosomal and apoptotic mechanism

Bacteria manipulate host cytoskeletal proteins for their mobility and distort the normal cytoskeleton. Few of the host cytoskeletal proteins including Actin-related protein 2 (Actr2), Alpha N-catenin (Ctnna2), Nucleolin (Ncl) were observed with an increased abundance change of 3.6-fold, 1.8-fold and 1.8-fold, respectively (Table S1). Under normal conditions, these proteins maintain the cytoskeletal homeostasis and the protein Actr2 is an ATP-binding component of the Arp2/3 complex that helps in cell motility by mediating the development of branching actin networks in the cytoplasm. The functioning of the Arp2/3 complex is required for vesicle trafficking, lamellipodium protrusion, and pathogen movement inside the host cell during infections. (18). Important proteins from lysosome pathway (KEGG ID: dre04142) showed a decreased trend in AH group (*Ah* infected). These include Cathepsin F-like protein (Ctsf, 3.7-fold decreased), Tripeptidyl-peptidase 1-like protein (Tpp1, 4.2-fold decreased), Lysosome membrane 2-like protein (Scarb2, 2.6-fold decreased) and Clathrin heavy chain (Cltca, 2.1-fold decreased). Different subunits of VATPase including Atp6voc, Atp6v1a, Atp8, Atp2b1 and palmitoyl-protein thioesterase 1 (Ppt1), Ras-related rab-15 (Rab15) and Ras-related Rab-1A (Rab1a) were also downregulated. Phospholipid scramblase 2-like (Plcsr3) which is a member of phospholipid scramblases, reported to mediate apoptosis by ATP independent bidirectional migration of phospholipids (19) has been observed with a 3.6-fold decreased abundance in *Ah* infected group (Table S1).

Another important protein, Glutathione-dependent dehydroascorbate reductase (Chuk) from apoptosis pathway was also found to be downregulated in AH group by 2.3-fold. Proteins from the immune system; Toll like receptor 3 (Tlr3) and C-type lectin domain family 4 member E-like protein (Clec4e/Cd207) and Chuk were found downregulated by 1.6, 1.9 and 2.3-fold, respectively, during the *Ah* infection. TLRs recognise pathogen-associated molecular patterns originating from microbes play a crucial function in macrophage maturation and activation and C-type lectins are also known to enhance adaptive immune responses (20).

Proteomic alterations related to immune functions, protein synthesis and Carbon metabolism

As expected, we observed significant increase in the host proteins belonging to proteosome and ubiquitin dependent degradation pathways (KEGG Pathway ID: dre03050) and B cell receptor (BCR) signalling, (Reactome Pathway ID: DRE-1168372) (Fig 3B). Many biological activities rely on ubiquitination, including transcriptional regulation, cell cycle progression, signal transduction, protein transport, immunological responses and pathogenesis. Bacterial infections may take advantage of the host's ubiquitin system to manipulate the immune response for their own benefits (21). Proteins like CCT-theta (Cct8), Intelectin 2 (Intl2), Proliferation-associated 2G4 (Pa2g4a), Galectin (Lgals3) and Unconventional myosin-Ic-like isoform X1 (Myo1c) which showed increased abundance in the *Ah* infected group, mapped to Innate immune system. Intelectin (Intl2) is a galectin binding lectin which has shown more than 6-fold increase during *Ah infection*. Intelectin has been shown to agglutinate bacteria, most likely due to its carbohydrate-binding ability, implying its role in innate immune system during the *Ah* infection (22). Also, the upregulated proteins such as subunits of proteasome; Psma8, Psma5, Psmd3, Psmd6, involved in downstream signaling events in BCR might be an indication of immune response during infection. Further, a panel of upregulated proteins mapped to ribosomal complex (viz. Rpl7a, Rps6, Rplp2, Rpl13), aminoacyl-tRNA biosynthesis

(viz. Qars, Eprs, Aars), and protein processing in endoplasmic reticulum (viz. Hsp90aa1, Rrbp1, Hspa8, Sec31a, Mogs). The increase in protein synthesis machinery during infections could be a modulated host response to maintain protein homeostasis and to promote host cell immune response against pathogen (23).

Proteins of carbon metabolism like 6-Phosphofructo-2-kinase (Pfk2), 2-Phospho-D-glycerate hydro-lyase (Eno1a), Citrate synthase (Cs), Succinyl-ligase (Suclg2), Acetyl-coenzyme A synthetase (Acss2) and oxidative phosphorylation (OXPHOS) as ATP synthase-coupling factor 6 (Atp5j), Inorganic diphosphatase (Ppa2), Complex -I proteins (Ndufa2, Ndufb10) were found to be increased during *Ah* infection in this study. Few proteins from OXPHOS including ATP synthase protein 8 (Atp8) and NADH Dehydrogenase (Ndufa6, Ndufb6, Ndufa12) were found to be control enriched and were not quantified in infected group. Also, proteins from fatty acid metabolism and peroxisome proliferator-activated receptors (PPAR) signaling pathways (viz. Fabp, Scp2, Cpt1) were upregulated in the *Ah* infected group. Alterations in Scp2 expression have been linked to several other liver functions such as bile acid metabolism, biliary lipid secretion, hepatic cholesterol storage and synthesis (24). PPAR signaling plays active role in regulating inflammatory responses in innate and adaptive immunity. The anti-inflammatory and antibacterial characteristics of PPAR activation may benefit the host during bacterial infections (25). Mineral and oxidant homeostasis was also altered during the *Ah* infection as a few related proteins such as Metalloreductase Steap4 (Steap4) and Glutamine gamma-glutamyltransferase (gGT) were upregulated in the *Ah* infected group. Stress response proteins including Heat shock HSP 90-alpha (Hsp90aa1) and Heat shock cognate 71 kDa (Hspa8) were also upregulated during the infection.

Targeted proteomic validation of dysregulated proteins using Selected Reaction Monitoring approach

The targeted proteomics data using SRM approach, was acquired for 27 differentially expressed proteins selected based on the discovery proteomics data (DDA followed by LFQ) (details in Methods section). The analysis ended up with a list of 328 transitions and 33 peptides belonging to sixteen proteins (plus 18 transitions for spiked in peptide) (Table S3). Nine proteins had at least two significant peptides. Group comparison analysis was performed in Skyline between 5 AH and 6 control samples which showed that the overall trend for these proteins is similar to that of DDA data in terms of increased or decreased abundance in *Ah* infected samples (AH condition) (AH condition) (Table S3). Among these, four proteins had three or more significant peptides passing the cut-off p value of 0.05 and fold change criterion of 1.5. These included three downregulated proteins viz. Bdh1 (D-beta-hydroxybutyrate mitochondrial), Chuk (D- Glutathione-dependent dehydroascorbate reductase) and Ugp2 (UTP-glucose-1-phosphate uridylyltransferase) (Fig. 4A-C) and one upregulated protein Atp5j (ATP synthase-coupling factor 6) (Fig. 4D). Individual sample wise peak area intensities for all the peptides of these proteins is represented in supplementary data (Fig. S3A-D, Table S3). Bdh1 is an important enzyme involved in lipid catabolism, Chuk protein has been reported for its role in apoptosis and Ugp2 is a carbon metabolic enzyme. Among the upregulated protein, the protein abundance changes were validated for Atp5j which is an important protein of oxidative phosphorylation. Additionally, five other proteins were found to be significant with 2 peptides only. These included three downregulated proteins namely, Dpys, Tpp1 and Sdr16c5, and two upregulated proteins ribosomal protein Rpl7a and Steap4 protein (Fig. S4).

DISCUSSION

Bacterial diseases are the most prominent cause of mass mortality in freshwater aquaculture system. Among the bacterial diseases, the disease caused by Aeromonas group has great significance. Proteomic analysis of liver tissue of *Aeromonas hydrophila (Ah)* infected *L. rohita* was performed to explore the perturbed proteins and pathways in *Ah* pathogenesis. This is the first comprehensive proteomic analysis carried out for liver tissue of *Ah* infected *L. rohita*. Pathway enrichment analysis of the upregulated and downregulated proteins revealed the involvement of these proteins in several biological processes that could provide insights for the pathogenesis of *Ah* infection. Our results summarised the key proteins and pathways involved in metabolic reprogramming of host cells during *Ah* infection. Pathways like lysosome pathway, apoptosis, metabolism of xenobiotics by cytochrome P450, retinol metabolism, pantothenate metabolism, beta alanine metabolism and drug metabolism were found to be majorly mapped by downregulated proteins. However, innate immune system, signaling of B cell receptor, proteosome pathway, ribosome, carbon metabolism and protein processing in ER were mainly mapped to upregulated proteins.

Our results showed a decrease in Biotinidase enzyme in liver tissue during *Ah* infection. Biotinidase is an important enzyme responsible for regeneration of biotin. In the head kidney, spleen, and skin of grass carp (*Ctenopharyngodon idella*), biotin deficiency lowered the mRNA levels of anti-microbial compounds (hepcidin, mucin and defensin), increased the levels of pro-inflammatory cytokines as interferon γ2 (IFN-γ2), interleukin 6 (IL-6), IL-1, IL-8 and tumour necrosis factor α (TNF-α) (15). During *Ah* infection, Antithrombin showed a decrease in *Ah* infected group compared to the control group. Besides its function in coagulation, antithrombin has been reported to exhibit anti-inflammatory responses against many gram negative and positive bacteria as it showed affinity to bind with lipopolysaccharide (LPS) on bacterial surfaces (16).

We observed that *Ah* infection affects the antioxidative and xenobiotic potential of the host. Liver is recognised as the primary site of detoxification and xenobiotic metabolism. Decreased protein abundance of several proteins was observed including few CYP proteins (Cyp1a, Cyp2f2, Cyp2g1, Cyp3a) related to xenobiotic metabolism and antioxidation, during *Ah* infection. Dysregulation of CYP genes was observed in channel catfish liver, gills and intestine after infection with *Edwardsiella ictaluri* where transcripts of several members of Cyp2 were downregulated as in our case (26). Monooxygenase Cyp1a protein which is downregulated in our study, showed an increase at transcriptomic level in the kidney, gill, testis and liver of Nile Tilapia after *Ah* infection (27). Proteins related to oxidative mechanism were decreased in AH group including Peroxidoxin 4 (Prdx4), Glutathione transferase, Glutathione peroxidase and Prenylcysteine oxidase 1. Our results for Prdx4 match with the report for human cell line samples where a proteome level decrease was observed in Prdx4 along with Prdx2 and Prdx6 after Lymphocytic Choriomeningitis Virus infection (28). We found a significant increase in the abundance of Steap4, a metalloreductase enzyme involved in iron and copper homeostasis. It is reported to play important role in cell responses to inflammatory and oxidative stresses and its expression can be modulated by hypoxia and cytokines such as IL-1 beta and TNF-alpha (29). Our results for Steap4 are similar to those reported in spleen of rainbow trout in response to *Yersinia ruckeri* infection (30). Such observations indicated an overall effect of *Ah* infection on general body functions and growth of fish through oxidative stress or dysregulation of its antioxidant capacity.

Our results suggest that *Ah* infection tends to affect the process of phagolysosomal killing by downregulating several proteins involved in the process. Proteins like Cathepsins, Tpp1, Ppt1 are cysteine and serine proteases or hydrolases that may play role in pathogen killing (31, 32). Vatpase enzymes are important for maintaining the acidic pH inside the lysosomes whereas the other proteins (as Rab proteins) are important for cargo transportation

344 inside the cell (33). Another protein, Phospholipid scramblase 2-like (Plcsr3) was observed
345 decreased during *Ah* infection. Plcsr3 has been reported to assist in the recognition of apoptotic
346 cells by macrophages (19). Alterations in these proteins could be the outcome of the pathogenic
347 processes that favor intracellular survival of the pathogen in the host cells (Fig. 5A).

348 Further we propose that *Ah* infection may promote the survival of infected cell by
349 escaping apoptosis or antimicrobial events by interfering with Tlr3 signaling. Immune related
350 protein, Tlr3 was found to be downregulated and another protein involved in the downstream
351 signaling; Dual specificity mitogen-activated kinase kinase 2-like protein (Map2k2b- MEK1/2)
352 was not detected in the infected group (Fig. 5B). TLRs, which recognise pathogen-associated
353 molecular patterns (PAMPs) arising from microorganisms, are one of the most important
354 components of innate or non-specific immunity (20). TLRs can stimulate the TIR-domain-
355 containing adapter-inducing interferon-dependent signaling pathway (TRIF) mediated
356 signaling through Tumor necrosis factor receptor–associated factor (TRAF) that finally
357 activates MAP kinase (MEK1/2), NF-κB or Activator protein (AP) (34). Tlr3 has generally
358 been recognised as endosomal receptor, whereas in *Labeo rohita* and *Cyprinus carpio,* it has
359 been reported as a cell surface receptor capable of TRIF mediated signaling (35). Tlr3, was the
360 first identified antiviral TLR member that has been reported to detect dsRNA of many RNA
361 viruses and activate the TIRF pathway, which produces type I interferon (IFN) and pro-
362 inflammatory cytokines (36). However, Tlr3 has also been observed to respond to bacterial
363 infection in zebrafish, channel catfish, yellow croaker and mice and to respond to Tlr2
364 microbial ligand peptidoglycan in immature dendritic cells (36). An increased level of Tlr3 at
365 transcriptomic level have been reported in Zebrafish in response to the infection with
366 *Edwardsiella tarda* (37). Our results are similar to those observed in kidney and spleen of blue
367 catfish (38) and kidney of rainbow trout (39) where Tlr3 expression was decreased after
368 infection with gram negative bacteria *E. ictulari* and *Yersinia ruckeri*, respectively. Also, Tlr3

369 downregulation has been related to immunosuppression in case of severe fever caused by Dabie
370 bandavirus (40). Tlr3 downregulation has been reported as a way to avoid apoptosis during
371 liver cancer (41, 42).

372 We observed a decreased abundance of Clec4e (Cd207) and Calcineurin in the *Ah*
373 infected group (Fig. 5B). Clec4e protein is a calcium-dependent lectin that acts as a pattern
374 recognition receptor (PRR) of the innate immune system and has been reported to be important
375 for autophagy and antimicrobial responses. Such C-type lectin receptor (CLRs) are known to
376 identify PAMPs and damage associated molecular patterns (DAMPs) and to activate NF-κB
377 signaling for the generation of cytokines and chemokines through the immune-receptor
378 tyrosine-based activation motif (ITAM) and SYK tyrosine kinase pathway (43). Clec4e has
379 been shown to cause signaling through Phospholipase C gamma 2 (PLCγ2) to activate the
380 calcineurin/NFAT pathway (43). Activated Calcineurin stimulates NFAT and NF-κB signaling
381 in T cells, regulates cell growth functions and apoptosis. The NFAT pathway is also involved
382 in the generation of antibodies and the differentiation of B cells (44). Decreased abundance of
383 Clec4e and Calcineurin indicates that *Ah* pathogenesis might involve Clec4e mediated
384 signaling to avoid antimicrobial effects and autophagy of the infected host cell. A combination
385 of Clec4e and Tlr4 agonists has been reported to inhibit the growth of *Mycobacterium*
386 *tuberculosis* in the lungs of *Mtb*-infected guinea pigs and mice (20). Similar
387 immunotherapeutic approach using Tlr3 can be designed for controlling *Ah* infection.

388 A few dysregulated proteins belong to Proteosome which is a protease complex
389 involved in hydrolysis of selected proteins in an ATP dependent manner. The proteasome
390 complex has been shown to regulate LPS-induced signal transduction, suggesting that it could
391 be a promising therapeutic target in Gram-negative bacteria. Alpha and beta subunits (Psma1
392 and Psmb4) of the 20S proteasome complex have been identified as LPS-binding proteins in
393 *Aeromonas salmonicida* infected rainbow trout (45). Further, mapping of upregulated proteins

394 to ribosomal subunits, ribosome biogenesis, amino acyl- tRNA complex and protein processing
395 in ER reveals an increased level of protein synthesis during *Ah* infection. Such biological
396 processes are essential for maintaining homeostasis and promoting host cell immune response
397 against pathogen during infections. Protein synthesis is also necessary for the survival of
398 bacteria inside the host, as reported in case of *Rhodopseudomonas palustris* infection (23).

399 Further we observed metabolic reprogramming of the host cells as a result of *Ah*
400 infection (Fig. 5C). Proteins related to energy metabolic processes including glycolysis, Kreb's
401 cycle, and oxidative phosphorylation have showed changes in response to *Ah* infection. Such a
402 reprogramming is more likely an adaptation to fulfil the high energetic and biosynthetic
403 demands in the infected host cell. Among the metabolic enzymes that were altered with *Ah*
404 infection, enzyme 6-Phosphofructo-2-kinase (Pfk2) showed an increased abundance. This
405 enzyme has been reported to play important role in maintaining glycolysis by allosterically
406 regulating the Phosphofructokinase 1 (Pfk1), a rate limiting enzyme of glycolysis (46). Another
407 glycolytic enzyme, Enolase (Eno1) is also upregulated in the AH group. Eno1 converts
408 phosphoglycerate to phosphoenolpyruvate that finally gives pyruvate. Another enzyme
409 involved in carbon metabolism (47); UTP--glucose-1-phosphate uridylyltransferase (Ugp2)
410 was also decreased by 1.7 folds which might be an indication of decreased glycogenesis in
411 support of glycolysis. Ugp2 is also reported to trigger immune responses through P2Y signaling
412 pathway (48). Upregulation of glycolytic enzymes could be a remodelling of the *Ah* infected
413 cell for cell proliferation, similar to what has been shown in cancer cells that rely on high rate
414 of glycolysis (49). Similar findings of glycolytic increase have been reported for mammalian
415 macrophages infected with *Mycobacterium tuberculosis (Mtb)* (50). Increase in the glycolytic
416 enzymes has been observed in kidney derived M1 macrophages of Carp upon activation with
417 bacterial LPS from *Escherichia coli* (51). M1 macrophages undergo metabolic reprogramming
418 from OXPHOS to glycolysis after activation with bacterial LPS alone or in conjunction with

IFN-γ (51). In *Mtb* infections, glycolytic reprogramming of M1 macrophages has been associated with two breaks in the tricarboxylic acid cycle (TCA cycle) and suppression of part of the electron transport chain (ETC) in the mitochondria. Breaks in TCA cycle includes the downregulation of two important enzymes i.e., Succinate dehydrogenase (SDH) and isocitrate dehydrogenase (IDH) that favours the build-up of Citrate and Succinate (52, 53).

These reported findings are complementary with our results as we could find higher expression of Acetyl-coenzyme A synthetase (Acss2), Citrate synthase (Cs) and Succinyl ligase (Suclg2) and a downregulation of Isocitrate dehydrogenase (IDH) which has shown enriched expression in the control group. Enzyme Cs catalyses the first reaction of TCA cycle where Oxaloacetate combines with Acetyl-CoA (involving Acss2) to form Citrate (Fig. 5C). The enzyme Succinyl ligase also known as Succinate synthase converts succinyl-CoA to Succinate and free coenzyme A. The downstream metabolite of Citrate (Itaconate) inhibits Succinate dehydrogenase (SDH) activity that again leads to an increase in Succinate (52). Both Citrate and Succinate have been reported to be involved in pro-inflammatory immune functions in macrophages. Citrate can accumulate in the cytosol to play important role in the production of mitochondrial reactive oxygen species (mROS), Nitric oxide (NO) and fatty acid synthesis. mROS can pose antimicrobial effects and activate interleukin 1 β (IL-1β) (54). Intracellular lipid metabolism promotes lipid droplet formation that are stored as energy resource for the cell required for inflammation, cell signaling and homeostasis. They can be utilised by the bacteria as well for promoting infection (55). In the later stages of infection, fatty acid metabolism may stimulate the peroxisome proliferator-activated receptor gamma (PPARγ) signaling which is known for its anti-inflammatory effects through inhibition of proinflammatory cytokines such as IL-1 *β and* TNF-*α* (56). Interestingly, we observed an increased expression of 15-oxoprostaglandin 13-reductase (Ptgr2) during *Ah* infection. Overexpression of Ptgr2 in the cells has been reported to decrease the PPARγ dependent

444 transcription (57). Moreover, Ptgr2 knockdown in LPS stimulated macrophages, resulted in
445 decreased production of pro-inflammatory cytokines (58). Such observations paved a way
446 towards exploring Ptgr2 mediated anti-inflammatory therapy for *Ah* infection. mROS can pose
447 antimicrobial effects and activate interleukin 1 β (IL-1β) (54).

448 Succinate accumulation also leads to the generation mROS and NO and can stabilise
449 hypoxia-inducible factor 1-alpha (HIF-1α). Activated HIF-1α further promotes the glycolytic
450 pathway and lactate production and causes inflammation by positively regulating the glycolytic
451 genes and IL-1β expression (52, 59). In our study, Lactate dehydrogenase enzyme (Ldha) has
452 been found to show enriched expression in the *Ah* infected group (AH group). During this
453 reprogramming, mitochondrial electron transport chain (ETC) is highly disturbed (52). In our
454 study, we observed dysregulation of many proteins involved in ETC and OXPHOS.
455 Dysregulated proteins include NADH dehydrogenase (Ndufa, Ndufb, Ndufv2, Ndufs8), ATP
456 synthase-coupling factor 6 (ATP5J), ATP synthase protein 8 (ATP8), Mt-co1(Cytochrome c
457 oxidase subunit 1), and Inorganic diphosphatase (Ppa2) (Fig. 5C). Such a reprogramming has
458 been profoundly observed in LPS activated dendritic cells and macrophages, activated effector
459 T cells, activated natural killer cells and activated B cells (60). Remodelling of these metabolic
460 processes enables the cells to produce sufficient ATP for performing cellular functions which
461 may be inflammatory cytokine production, phagocytosis or antigen presentation (60). Based
462 on these findings and our observations, we hypothesise that *Ah* pathogenesis in *Labeo rohita*
463 involves metabolic reprogramming that supports several inflammatory immune functions
464 which is a hallmark for most immune cells.

465

466

467

CONCLUSIONS

We analysed the proteome level dynamics in liver tissue of *L. rohita* as a result of *Ah* infection. Our proteomics analysis provided new insights into the proteins involved and processes underlying *Ah* pathogenesis in *L. rohita.* We observed that during *Ah* infection, several host proteins and metabolic pathways were altered affecting important biological processes like antioxidative potential, lysosomal killing and apoptosis. We also observed remodelling of important energy related processes such as glycolysis and Krebs cycle which might be useful in modulating inflammatory response during *Ah* infection in *L. rohita*. Our findings have cleared the way for more research into the involvement of Toll-like receptors (Tlr3), C-type lectins (Clec4e), and metabolic enzymes in *Ah* pathogenesis. Collectively, our data provided new mechanistic insights into *Ah* infection that can help in characterisation of host-pathogen interactions and aid in the selection and prioritisation of proteins to be used in host directed immunotherapy against *Ah* infection.

MATERIALS AND METHODS

Overall experimental design

This study aimed at proteomic profiling of liver tissue of *Ah* infected *Labeo rohita*. Fishes were challenged with *Ah* and sampled such that there was a total of 12 samples including six each for Control and AH group (*Ah* infected). Following sample collection, discovery based proteomic analysis was performed by taking four samples for each group (four each of Control and AH group). The data was analyzed using MaxQuant software followed by statistical analysis in Metaboanalyst tool to identify the differentially expressed proteins (DEPs) in liver tissue. Gene ontology (GO) analysis was performed to obtain an overview of functional annotation of significant proteins and dysregulated metabolic pathways. The protein abundance changes for a panel of differentially expressed proteins was validated using SRM approach where eleven samples (6 Control and 5 AH) were analyzed. Further, detailed analysis was done to understand the molecular mechanism of *Ah* infection.

Bacterial collection and identification

In the study, *Aeromonas hydrophila* strain was isolated from the kidney tissue of naturally co-infected *Labeo rohita* (NCBI Accession no. MT374248). Briefly, kidney tissue was streaked onto tryptic soy agar (TSA, Himedia) and incubated at 28 ℃ for 24 hours. Representative colonies were isolated and re-streaked on fresh TSA medium until purity was attained. Pure cultures of the isolated bacteria were subjected to morphological analysis, and the taxonomy of the isolates was determined following the 16S rRNA gene using the gene sequence universal primers; forward primer 27F 5'-AGAGTTTGATCCTGGCTCAG-3' and reverse primer 1492R 5'- GGTTACCTTGTTACGACTT-3' (Chromous Biotech Ltd., Bengaluru, India) (61) (Fig. 1A). The strain was stored at −70 °C in 30% glycerol stock until use for the challenge study.

514 To detect the virulence of strain, *Ah* (MT374248) was cultured in Brain Heart Infusion broth
515 (BHI) (Himedia) at 28 ℃ and kept in incubator at 150 rpm for 18 hours. For confirmation of
516 *Ah*, a loop of bacteria was streaked onto Aeromonas Isolation Medium HiVegTM Base
517 (Himedia) and polymerase chain reaction (PCR) was conducted using target segments of
518 primers; forward: 16S rDNA1 451–473 5′-GAAAGGTTGATGCCTAATACGTA-3′ and
519 reverse:16S DNA2 1115–1135 5′-CGTGCTGGCAACAAAGGACAG-3′ with an expected
520 product length of 685 bp (62). The amplifications were performed in thermal cycler (Bio-Rad,
521 USA) in which 30 PCR cycles were run under the following conditions; denaturation at 94 ℃
522 for 2 min, primer annealing at 56 ℃ for 2 min, and DNA extension at 72 ℃ for 2 min in each
523 cycle. A negative control with all the reaction components except template DNA and a positive
524 control (extracted genomic DNA, from *Ah* MTCC culture, 1739T- Chandigarh, India) were
525 considered. Ten microliters of PCR products were electrophoresed in a 1% agarose gel
526 containing ethidium bromide at 100 V for 1 hour, visualized on an ultraviolet (UV)
527 transilluminator (Bio-Rad) (Fig. S5).

528 **Collection of fish and maintenance for the experiment**

529 For expression study, six-month-old fish (N=150, average weight 70±10 g) were collected from
530 a local fish farm (Pen Raigad District, Maharashtra) and brought to wet lab facility (ICAR-
531 CIFE, Mumbai). Fishes were equally distributed and acclimated in three circular fibre tanks
532 and fed 2 % body weight. Fishes were maintained at a temperature of 26-28 ℃ with proper
533 aeration, and removal of faeces on daily basis. All the fishes were observed for external clinical
534 signs and randomly few fishes from three tanks sacrificed to observe pathogen in the fish using
535 PCR.

536 ***Aeromonas hydrophila* challenge and sampling**

537 For challenge test, LD50 dose was determined as per the protocol described by
538 Siriyappagouder et al. (63) and found to be 1.5×10^8 CFU for the isolated strain. The bacteria

were cultured till 18 hours, and LD50 dose of 1.5 $\times 10^8$ CFU suspension was prepared after washing with PBS. The fish were pooled and acclimatized, starved for 2 days and then approximately 1.5×10^8 bacterial cells in PBS or the same volume of PBS solution (Control) were intraperitoneally inoculated into 36 fish (18 each for control and challenged). The challenged and control groups were separately maintained in six crates (6 fish each) of a 100-liter capacity high density polyethylene plastic crate at 26-28 °C. The presence of external signs of hemorrhage were observed in the challenged fish groups post-infection. Expectedly, these signs were not detected in the control group (Fig. S6). After 48 hours, fish were euthanized and liver samples were collected. Collected samples were stored at -80 C till further use. For proteomic analysis, tissue from three fishes were pooled into one resulting in a total of six samples each for control and challenged group labelled as Liv-C1 to C6 and Liv-AH1 to AH6, respectively.

Tissue lysis and protein extraction

Tissue lysates were prepared using SDS containing lysis buffer (5% SDS, 100mM Tris/HCl pH 8.5 (adjusted with phosphoric acid). The tissue was weighed (40-50 mg) and rinsed in a 1X phosphate buffered saline (PBS) solution (2-3 times to remove any blood). After washing the tissue, 250 µl of lysis buffer was added to the tissue along with 5 µl of Protease inhibitor cocktail (50X stock, Sigma- Catalogue no. 11873580001) and incubated on ice for 30 min. Sonication was performed for 2 min with an amplitude of 40% with 5 sec pulse on and 5 sec off. Centrifugation was done to remove the debris and clear supernatant was collected.

Protein quantification and digestion

Tissue lysates were processed for quantification of proteins using the BCA assay (Thermo, Ref. 23227) with Bovine serum albumin as the standard protein. After quantification, 30 µg protein was taken for digestion using filter assisted sample preparation (FASP) based digestion method. In brief, the protein was first reduced using TCEP solution with a final concentration

of 20 mM. Initial volume at this step was kept as 30 µl (volume made up using 1X lysis buffer). Reduced sample was loaded onto a 30 KDa filter (Catalogue no. MRCF0R030- Merck Millipore) to proceed for FASP based digestion. Following the required steps of alkylation and washing, trypsin mixed in digestion buffer (50 mM Ammonium Bicarbonate) was added in 1:30 ratio for enzyme to protein. Samples were incubated in a wet chamber at 37°C for 16 hours. Digested peptides were eluted in a fresh collection tube, dried and stored until further processing. Before mass spectrometry, samples were cleaned using C18 stage tips (Empore™ SPE Disks matrix active group C18, diam. 47 mm, catalogue no. 66883-U- Merck).

Liquid chromatography tandem mass spectrometry in data dependent acquisition mode

For all the samples, peptides were quantified using Scopes method (64). After quantification, one µg of peptide sample was loaded on the column and LC-MS/MS was performed. All samples (4 for each Control and AH group) were run with an LC gradient of 120 min. Data was acquired using an Orbitrap-Fusion Tribrid mass-spectrometer connected to an Easy-nLC nano-flow liquid chromatography 1200 system. Peptide sample was loaded onto the pre-analytical column (100 µm x 2 cm, nanoViper C18, 5 µm, 100A; Thermo Fisher Scientific) at a flow rate of 5 µl/min. Peptides were resolved on analytical column (75 µm × 50 cm, 3 µm particle, and 100 Å pore size; Thermo Fisher Scientific) at a flow rate of 300 nl/min over 120 min gradient in solvent B (80% Acetonitrile with 0.1% Formic acid (FA). The Orbitrap mass analyzer was used to perform mass spectrometric acquisition in data dependent acquisition (DDA) mode in the full scan range of 375-1700 m/z with a mass resolution of 60,000. With a dynamic exclusion time of 40 seconds, the mass window was set at 10 ppm. All MS/MS spectra were obtained using the HCD method (High Energy Collision Dissociation) for fragmentation at MS1 and MS2 level, the AGC target was set at 400000 and 10000, respectively. A lock mass of 445.12003 m/z was used for positive internal calibration.

Protein identification and quantification using label-free quantification approach

589 The raw mass spectrometry data was analysed using MaxQuant (v1.6.6.0) software against
590 UniProt protein database for *Labeo rohita* (ProteomeID- UP000290572, Taxonomy ID- 84645,
591 downloaded on 18.06.2021) using the in-built search engine, Andromeda. All the raw files
592 were analyzed together using Label-Free-Quantification (LFQ) parameters. Label type was set
593 to standard with a multiplicity of 1, and the match between run option was checked. Orbitrap
594 fusion mode was selected as instrument, and trypsin as a protease was chosen. A total of two
595 missed cleavages were permitted. Carbamidomethylation at Cysteine (+57.021464 Da) was
596 chosen for fixed modification, and oxidation at Methionine (+15.994915 Da) was chosen for
597 variable modification. A false discovery rate of 1% was specified for both proteins and
598 peptides. Reverse was chosen as the decoy mode option, and proteins were recognised solely
599 by their unique peptide. The LFQ intensities obtained for each sample were considered for
600 quantitative analysis (Table S1).

601 **Statistical analysis using MetaboAnalyst**

602 Statistical analysis was performed taking MaxQuant analyzed files in Metaboanalyst software
603 (65). One of the samples (Liv-AH1) was discarded due to poor mass spectrometry results (Fig.
604 S1A) The proteomic data of the remaining seven samples was considered for further analysis
605 including four Control samples; Liv-C1, 2, 3, 4 and three *Ah* infected samples (AH group)
606 labelled as Liv-AH2, 3, 4. The K-Nearest Neighbor (KNN) algorithm was used to impute the
607 missing values of proteins with abundance values in more than 75% of each group, which were
608 then used in differential protein expression analysis. The data was $\log_{10}$ transformed before
609 further statistical analysis. The significant differentially expressed proteins were identified
610 using a two-sample t-test (Welch t-test) with a p-value threshold of 0.05. Proteins with
611 minimum fold change value of 1.5 were regarded as significant differentially expressed
612 proteins (DEPs) among all t-test passed proteins. Variable importance in projection (VIP) score
613 was obtained through Partial Least Squares Discriminant Analysis (PLS-DA) which is a

supervised method. As a weighted sum of squares of the PLS weight, VIP indicates the importance of the variable to the whole model. Heatmap representing the expression of top DEPs was also obtained from Metaboanalyst analysis. Volcano plots were plotted using online tool VolcanoseR (66).

Gene ontology, Pathway and protein-protein interaction enrichment analysis

Selected dysregulated proteins obtained from LFQ data were taken forward for functional annotation and biological pathway analysis. Gene names of dysregulated proteins were retrieved from EggNOG resource (67) on the basis of ortholog annotation and from literature (as the gene names for *L. rohita* are not updated yet in the available databases). The protein-protein interaction (PPI) enrichment analysis and visualization of their involvement in respective biological pathways (KEGG and Reactome) was performed using STRING tool version 11.5 (68) taking genes of significantly upregulated and downregulated proteins as input (Table S2). *Danio rerio* was selected as reference organism as these databases are not yet updated for *Labeo rohita*. Furthermore, biological functional pathway enrichment of different Gene Ontologies (GO), KEGG, Reactome and Panther Pathway and PPI were done using Metascape tool (69). In Metascape, custom analysis of DEPs, control and disease enriched proteins were performed selecting *Danio rerio* as reference organism, considering all of the terms and categories for annotation and membership (Table S2). Minimum overlap of 3, p-value cut off of 0.05, minimum enrichment 1.5 were taken as parameters for pathway and process enrichment and physical core database was selected for protein-protein interaction enrichment analysis.

Targeted proteomic validation of dysregulated proteins using SRM approach

For acquiring the targeted proteomic data using selected/ multiple reaction monitoring (SRM/MRM) approach, TSQ Altis mass spectrometer (ThermoFisher Scientific, USA) coupled to an HPLC-Dionex Ultimate 3000 system (ThermoFisher Scientific, USA) was used.

In order to separate the peptides, a Hypersil Gold C18 column (1.9 µm, 100 x 2.1 mm, ThermoFisher Scientific, USA) was used. The flow rate was maintained as 0.45 ml/min for 10 min. Solutions of 0.1% FA and 80% ACN in 0.1% FA were taken as buffer A and B, respectively in the binary buffer system. The gradient used for chromatographic separation of the peptides was as follows; 2-45% buffer B for first 6 min, 45-95% buffer B for 0.5 min, 95% buffer B for 0.5 min, 95%-2% buffer B for 0.5 min, and 2% buffer B for 2.5 min.

We started with a list of 30 proteins (16 upregulated and 17 downregulated) corresponding to 244 peptides and ~4000 transitions. The Skyline software, version 20.1.1.196 (70) was used to prepare the transition lists to be fed into the system. The criteria included for miss cleavage was 0, for precursor charges +2, +3, and product charge was +1 with 'y' ion transitions (from ion 2 to last ion -1). A background proteome consisting of UniProt protein database for *Labeo rohita* (ProteomeID- UP000290572, Taxanomy ID- 84645, downloaded on 18.06.2021) was used. Unique peptides previously identified in the discovery data were only selected for the targeted experiment. The collision energy values used in the experiment were as determined by Skyline software. One µg of peptides from each sample were injected and run against the target list. Initial optimization was done using pooled peptide samples which were run against nine transition lists each with 400-450 transitions per method. Consequently, the list was refined based on consistency of the spectral data. Before injecting to mass spectrometer, all the samples were spiked in with equal amount or heavy labelled synthetic peptide DIFTGLIGPMK (C-terminus lysine labelled). Synthetic peptide was added to monitor the consistency of the mass spectrometric run, for which 18 transitions were added to the final transition list. For the final SRM run, the data was acquired for all the samples (five AH and six Control) using two transition lists (two SRM methods) consisting of 617 transitions and 91 peptides corresponding to 27 proteins resulting in 22 raw files (Table S3).

Targeted proteomics data analysis

After data acquisition, all the downstream data analysis was performed in Skyline software (70). MSMS (.msms) file obtained from the Maxquant analysis was utilised for preparing the DDA spectral library for analysing S/MRM data. The result files (.raw) were imported to the Skyline software and assigned to respective conditions as Control and AH. Each peptide was manually annotated based on peak shape and retention time alignment with other replicates of the same peptide and library match (dot product measurement). The peptides that didn't adhere well to the retention time alignment were deleted after manual annotation to refine the data. Statistical analysis was performed using MSstats external tool inbuilt in Skyline in which certain peptides were found after the fold change analysis (cut off 1.5) with significant p-value (0.05). Result reports for all the peptides containing their peak area values were exported in .csv format to carry out the further analysis (Table S3). Further data analysis was done for proteins with two or more significant peptides and violin plots for peptide wise intensities (Table S3) were created using an online tool BoxPlotR (71).

DATA AVAILABILITY

The protein database (.FASTA) and raw mass spectrometry data (.raw) have been deposited to the ProteomeXchange Consortium via the PRIDE partner repository. All result output files for protein identification are also submitted in text (.text) format along with the parameter file. Also, the spectral library (.blib) generated using the discovery data for analysing the targeted data is uploaded. The identifier PXD029421 can be used to retrieve all of the data. (Reviewer account details: Username: reviewer_pxd029421@ebi.ac.uk, Password: lI191yU0).

The transition lists, skyline documents, and all SRM raw (.raw) data for the Selected reaction monitoring (SRM) experiment have been submitted to Panorama public that can be accessed through the given link https://panoramaweb.org/rohuliverproteomicsah.url

(Reviewer account details: panorama+reviewer75@proteinms.net Password: OKRYbqkf).

AUTHOR'S CONTRIBUTIONS

Concept and design: M.N., S.S. and M.G.

Maintenance and sampling: N.P., M.N. and M.G.

Method development and Data acquisition: M.N. and S.S

Data analysis and Interpretation: M.N., N.P., B.G. and U.S.

Writing and review: M.N., N.P., B.G., U.S., M.G. and S.S

ACKNOWLEDGEMENTS

This work was supported by Department of Biotechnology (BT/PR15285/AAQ/3/753/2015) Govt. of India to S.S and M.G. M.N was supported by University Grants Commission (UGC). We acknowledge ICAR-Central Institute of Fisheries Education, Mumbai for supporting this work. We acknowledge MASS-FIITB at IIT Bombay supported by the Department of Biotechnology (BT/PR13114/INF/22/206/2015) for Mass-spectrometric data acquisition.

SUPPLEMENTAL INFORMATION

This article contains six supplementary figures (Figure S1 to S6) and three supplementary Tables (Table S1 to S3) (.xls).

REFERENCES

1. Assefa A, Abunna F. 2018. Maintenance of Fish Health in Aquaculture: Review of Epidemiological Approaches for Prevention and Control of Infectious Disease of Fish. Vet Med Int 2018:5432497.

2. Sahoo PK, Paul A, Sahoo MK, Sabyasachi P, P RK, Das BK. 2021. Incidences of Infectious Diseases in Freshwater Aquaculture Farms of Eastern India: A Passive Surveillance based Study from 2014-2018. J Aquac Res Dev 11:579.

3. Bebak J, Wagner B, Burnes B, Hanson T. 2015. Farm size, seining practices, and salt use: Risk factors for Aeromonas hydrophila outbreaks in farm-raised catfish, Alabama, USA. Preventive Veterinary Medicine 118:161–168.

4. Abdel-Latif HMR, Khafaga AF. 2020. Natural co-infection of cultured Nile tilapia *Oreochromis niloticus* with *Aeromonas hydrophila* and *Gyrodactylus cichlidarum* experiencing high mortality during summer. Aquac Res 51:1880–1892.

5. Dias MKR, Sampaio LS, Proietti-Junior AA, Yoshioka ETO, Rodrigues DP, Rodriguez AFR, Ribeiro RA, Faria FSEDV, Ozório ROA, Tavares-Dias M. 2016. Lethal dose and clinical signs of Aeromonas hydrophila in Arapaima gigas (Arapaimidae), the giant fish from Amazon. Vet Microbiol 188:12–15.

6. Najiah M LA. 2014. Aeromonas hydrophila: Antimicrobial Susceptibility and Histopathology of Isolates from Diseased Catfish, Clarias gariepinus (Burchell). J Aquac Res Development 05.

7. Zhao X-L, Jin Z-H, Di G-L, Li L, Kong X-H. 2019. Molecular characteristics, pathogenicity and medication regimen of Aeromonas hydrophila isolated from common carp (Cyprinus carpio L.). J Vet Med Sci 81:1769–1775.

8. Pérez-Llarena FJ, Bou G. 2016. Proteomics As a Tool for Studying Bacterial Virulence and Antimicrobial Resistance. Frontiers in Microbiology 7:410.

9. Zhang L, Li W, Sun L, Wang Y, Lin Y, Lin X. 2020. Quantitative proteomics reveals the molecular mechanism of Aeromonas hydrophila in enoxacin stress. J Proteomics 211:103561.

10. Di G, Li H, Zhang C, Zhao Y, Zhou C, Naeem S, Li L, Kong X. 2017. Label-free proteomic analysis of intestinal mucosa proteins in common carp (Cyprinus carpio) infected with Aeromonas hydrophila. Fish Shellfish Immunol 66:11–25.

11. Zhang H, Song C, Xie J, Ge X, Liu B, Zhang Y, Sun C, Zhou Q, Yang Z. 2018. Comparative proteomic analysis of hepatic mechanisms of Megalobrama amblycephala infected by Aeromonas hydrophila. Fish Shellfish Immunol 82:339–349.

12. Lü A, Hu X, Wang Y, Shen X, Li X, Zhu A, Tian J, Ming Q, Feng Z. 2014. iTRAQ analysis of gill proteins from the zebrafish (Danio rerio) infected with Aeromonas hydrophila. Fish Shellfish Immunol 36:229–239.

13. Magnadottir B. 2010. Immunological control of fish diseases. Mar Biotechnol (NY) 12:361–379.

14. Heymann F, Tacke F. 2016. Immunology in the liver--from homeostasis to disease. Nat Rev Gastroenterol Hepatol 13:88–110.

15. He P, Jiang W-D, Liu X-A, Feng L, Wu P, Liu Y, Jiang J, Tan B-P, Yang Q-H, Kuang S-Y, Tang L, Zhou X-Q. 2020. Dietary biotin deficiency decreased growth performance and impaired the immune function of the head kidney, spleen and skin in on-growing grass carp (Ctenopharyngodon idella). Fish Shellfish Immunol 97:216–234.

16. Schlömmer C, Brandtner A, Bachler M. 2021. Antithrombin and Its Role in Host Defense and Inflammation. Int J Mol Sci 22:4283.

17. Al-Madboly LA, Ali SM, Fakharany EME, Ragab AE, Khedr EG, Elokely KM. 2020. Stress-Based Production, and Characterization of Glutathione Peroxidase and Glutathione S-Transferase Enzymes From Lactobacillus plantarum. Front Bioeng Biotechnol 8:78.

18. Rottner K, Stradal TEB. 2016. How distinct Arp2/3 complex variants regulate actin filament assembly. Nat Cell Biol 18:1–3.

19. Kodigepalli KM, Bowers K, Sharp A, Nanjundan M. 2015. Roles and regulation of phospholipid scramblases. FEBS Lett 589:3–14.

20. Pahari S, Negi S, Aqdas M, Arnett E, Schlesinger LS, Agrewala JN. 2020. Induction of autophagy through CLEC4E in combination with TLR4: an innovative strategy to restrict the survival of *Mycobacterium tuberculosis*. Autophagy 16:1021–1043.

21. Kim M, Otsubo R, Morikawa H, Nishide A, Takagi K, Sasakawa C, Mizushima T. 2014. Bacterial effectors and their functions in the ubiquitin-proteasome system: insight from the modes of substrate recognition. Cells 3:848–864.

22. Chen L, Li J, Yang G. 2020. A comparative review of intelectins. Scandinavian Journal of Immunology 92:e12882.

23. Yin L, Ma H, Nakayasu ES, Payne SH, Morris DR, Harwood CS. 2019. Bacterial Longevity Requires Protein Synthesis and a Stringent Response. mBio 10:e02189-19.

24. Zanlungo S, Amigo L, Mendoza H, Miquel JF, Vío C, Glick JM, Rodríguez A, Kozarsky K, Quiñones V, Rigotti A, Nervi F. 2000. Sterol carrier protein 2 gene transfer changes lipid metabolism and enterohepatic sterol circulation in mice. Gastroenterology 119:1708–1719.

25. Bedi B, Maurice NM, Ciavatta VT, Lynn KS, Yuan Z, Molina SA, Joo M, Tyor WR, Goldberg JB, Koval M, Hart CM, Sadikot RT. 2017. Peroxisome proliferator-activated receptor-γ agonists attenuate biofilm formation by Pseudomonas aeruginosa. FASEB J 31:3608–3621.

26. Zhang J, Yao J, Wang R, Zhang Y, Liu S, Sun L, Jiang Y, Feng J, Liu N, Nelson D, Waldbieser G, Liu Z. 2014. The cytochrome P450 genes of channel catfish: Their involvement in disease defense responses as revealed by meta-analysis of RNA-Seq data sets. Biochimica et Biophysica Acta (BBA) - General Subjects 1840:2813–2828.

817 27. Hal AM, El-Barbary MI. 2020. Gene expression and histopathological changes of Nile
818 tilapia (Oreochromis niloticus) infected with Aeromonas hydrophila and Pseudomonas
819 fluorescens. Aquaculture 526:735392.

820 28. Benej M, Danchenko M, Oveckova I, Cervenak F, Tomaska L, Grossmannova K,
821 Polcicova K, Golias T, Tomaskova J. 2019. Quantitative Proteomics Reveal
822 Peroxiredoxin Perturbation Upon Persistent Lymphocytic Choriomeningitis Virus
823 Infection in Human Cells. Frontiers in Microbiology 10:2438.

824 29. Scarl RT, Lawrence CM, Gordon HM, Nunemaker CS. 2017. STEAP4: its emerging
825 role in metabolism and homeostasis of cellular iron and copper. Journal of
826 Endocrinology 234:R123–R134.

827 30. Kumar G, Hummel K, Noebauer K, Welch TJ, Razzazi-Fazeli E, El-Matbouli M. 2018.
828 Proteome analysis reveals a role of rainbow trout lymphoid organs during Yersinia
829 ruckeri infection process. Sci Rep 8:13998.

830 31. Newton P, Thomas DR, Reed SCO, Lau N, Xu B, Ong SY, Pasricha S,
831 Madhamshettiwar PB, Edgington-Mitchell LE, Simpson KJ, Roy CR, Newton HJ. 2020.
832 Lysosomal degradation products induce Coxiella burnetii virulence. Proc Natl Acad Sci
833 U S A 117:6801–6810.

834 32. Szulc-Dąbrowska L, Bossowska-Nowicka M, Struzik J, Toka FN. 2020. Cathepsins in
835 Bacteria-Macrophage Interaction: Defenders or Victims of Circumstance? Front Cell
836 Infect Microbiol 10:601072.

837 33. Schwartz SL, Cao C, Pylypenko O, Rak A, Wandinger-Ness A. 2008. Rab GTPases at a
838 glance. Journal of Cell Science 121:246–246.

839 34. Ullah MO, Sweet MJ, Mansell A, Kellie S, Kobe B. 2016. TRIF-dependent TLR
840 signaling, its functions in host defense and inflammation, and its potential as a
841 therapeutic target. Journal of Leukocyte Biology 100:27–45.

842 35. Samanta M, Basu M, Swain B, Panda P, Jayasankar P. 2013. Molecular cloning and
843 characterization of Toll-like receptor 3, and inductive expression analysis of type I IFN,
844 Mx and pro-inflammatory cytokines in the Indian carp, rohu (Labeo rohita). Mol Biol
845 Rep 40:225–235.

846 36. Lin K, Ge H, Lin Q, Wu J, He L, Fang Q, Zhou C, Sun M, Huang Z. 2013. Molecular
847 characterization and functional analysis of Toll-like receptor 3 gene in orange-spotted
848 grouper (Epinephelus coioides). Gene 527:174–182.

849 37. Meijer AH, Gabby Krens SF, Medina Rodriguez IA, He S, Bitter W, Ewa Snaar-
850 Jagalska B, Spaink HP. 2004. Expression analysis of the Toll-like receptor and TIR
851 domain adaptor families of zebrafish. Mol Immunol 40:773–783.

852 38. Baoprasertkul P, Peatman E, Somridhivej B, Liu Z. 2006. Toll-like receptor 3 and
853 TICAM genes in catfish: species-specific expression profiles following infection with
854 Edwardsiella ictaluri. Immunogenetics 58:817–830.

855 39. Rodriguez MF, Wiens GD, Purcell MK, Palti Y. 2005. Characterization of Toll-like
856 receptor 3 gene in rainbow trout (Oncorhynchus mykiss). Immunogenetics 57:510–519.

40. Song P, Zheng N, Zhang L, Liu Y, Chen T, Bao C, Li Z, Yong W, Zhang Y, Wu C, Wu Z. 2017. Downregulation of Interferon-β and Inhibition of TLR3 Expression are associated with Fatal Outcome of Severe Fever with Thrombocytopenia Syndrome. Sci Rep 7:6532.

41. Bonnin M, Fares N, Testoni B, Estornes Y, Weber K, Vanbervliet B, Lefrançois L, Garcia A, Kfoury A, Pez F, Coste I, Saintigny P, Viari A, Lang K, Guey B, Hervieu V, Bancel B, Bartoch B, Durantel D, Renno T, Merle P, Lebecque S. 2019. Toll-like receptor 3 downregulation is an escape mechanism from apoptosis during hepatocarcinogenesis. J Hepatol 71:763–772.

42. Yuan M-M, Xu Y-Y, Chen L, Li X-Y, Qin J, Shen Y. 2015. TLR3 expression correlates with apoptosis, proliferation and angiogenesis in hepatocellular carcinoma and predicts prognosis. BMC Cancer 15:245.

43. Drouin M, Saenz J, Chiffoleau E. 2020. C-Type Lectin-Like Receptors: Head or Tail in Cell Death Immunity. Front Immunol 11:251.

44. Park Y-J, Yoo S-A, Kim M, Kim W-U. 2020. The Role of Calcium-Calcineurin-NFAT Signaling Pathway in Health and Autoimmune Diseases. Front Immunol 11:195.

45. Long M, Zhao J, Li T, Tafalla C, Zhang Q, Wang X, Gong X, Shen Z, Li A. 2015. Transcriptomic and proteomic analyses of splenic immune mechanisms of rainbow trout (Oncorhynchus mykiss) infected by Aeromonas salmonicida subsp. salmonicida. J Proteomics 122:41–54.

46. Ros S, Schulze A. 2013. Balancing glycolytic flux: the role of 6-phosphofructo-2-kinase/fructose 2,6-bisphosphatases in cancer metabolism. Cancer & Metabolism 1:8.

47. Wolfe AL, Zhou Q, Toska E, Galeas J, Ku AA, Koche RP, Bandyopadhyay S, Scaltriti M, Lebrilla CB, McCormick F, Kim SE. 2021. UDP-glucose pyrophosphorylase 2, a regulator of glycogen synthesis and glycosylation, is critical for pancreatic cancer growth. PNAS 118.

48. Ma J, Wei K, Liu J, Tang K, Zhang H, Zhu L, Chen J, Li F, Xu P, Chen J, Liu J, Fang H, Tang L, Wang D, Zeng L, Sun W, Xie J, Liu Y, Huang B. 2020. Glycogen metabolism regulates macrophage-mediated acute inflammatory responses. Nat Commun 11:1769.

49. Vaupel P, Schmidberger H, Mayer A. 2019. The Warburg effect: essential part of metabolic reprogramming and central contributor to cancer progression. Int J Radiat Biol 95:912–919.

50. Shi L, Salamon H, Eugenin EA, Pine R, Cooper A, Gennaro ML. 2015. Infection with Mycobacterium tuberculosis induces the Warburg effect in mouse lungs. Sci Rep 5:18176.

51. Wentzel AS, Janssen JJE, de Boer VCJ, van Veen WG, Forlenza M, Wiegertjes GF. 2020. Fish Macrophages Show Distinct Metabolic Signatures Upon Polarization. Frontiers in Immunology 11:152.

896 52. Park J-H, Shim D, Kim KES, Lee W, Shin SJ. 2021. Understanding Metabolic
897 Regulation Between Host and Pathogens: New Opportunities for the Development of
898 Improved Therapeutic Strategies Against Mycobacterium tuberculosis Infection.
899 Frontiers in Cellular and Infection Microbiology 11:212.

900 53. Williams NC, O'Neill LAJ. 2018. A Role for the Krebs Cycle Intermediate Citrate in
901 Metabolic Reprogramming in Innate Immunity and Inflammation. Frontiers in
902 Immunology 9:141.

903 54. Gleeson LE, Sheedy FJ. 2016. Metabolic reprogramming & inflammation: Fuelling the
904 host response to pathogens. Semin Immunol 28:450–468.

905 55. Libbing CL, McDevitt AR, Azcueta R-MP, Ahila A, Mulye M. 2019. Lipid Droplets: A
906 Significant but Understudied Contributor of Host¯Bacterial Interactions. Cells 8:E354.

907 56. Reddy AT, Lakshmi SP, Reddy RC. 2016. PPARγ in Bacterial Infections: A Friend or
908 Foe? PPAR Research 2016:e7963540.

909 57. Chou W-L, Chuang L-M, Chou C-C, Wang AH-J, Lawson JA, FitzGerald GA, Chang
910 Z-F. 2007. Identification of a novel prostaglandin reductase reveals the involvement of
911 prostaglandin E2 catabolism in regulation of peroxisome proliferator-activated receptor
912 gamma activation. J Biol Chem 282:18162–18172.

913 58. Chen I-J, Hee S-W, Liao C-H, Lin S-Y, Su L, Shun C-T, Chuang L-M. 2018. Targeting
914 the 15-keto-PGE2-PTGR2 axis modulates systemic inflammation and survival in
915 experimental sepsis. Free Radical Biology and Medicine 115:113–126.

916 59. Tannahill GM, Curtis AM, Adamik J, Palsson-McDermott EM, McGettrick AF, Goel G,
917 Frezza C, Bernard NJ, Kelly B, Foley NH, Zheng L, Gardet A, Tong Z, Jany SS, Corr
918 SC, Haneklaus M, Caffrey BE, Pierce K, Walmsley S, Beasley FC, Cummins E, Nizet
919 V, Whyte M, Taylor CT, Lin H, Masters SL, Gottlieb E, Kelly VP, Clish C, Auron PE,
920 Xavier RJ, O'Neill L a. J. 2013. Succinate is an inflammatory signal that induces IL-1β
921 through HIF-1α. Nature 496:238–242.

922 60. O'Neill LAJ, Kishton RJ, Rathmell J. 2016. A guide to immunometabolism for
923 immunologists. Nat Rev Immunol 16:553–565.

924 61. Stackebrandt E, Goebel BMY 1994. 1994. Taxonomic Note: A Place for DNA-DNA
925 Reassociation and 16S rRNA Sequence Analysis in the Present Species Definition in
926 Bacteriology. International Journal of Systematic and Evolutionary Microbiology
927 44:846–849.

928 62. Chu W-H, Lu C-P. 2005. Multiplex PCR assay for the detection of pathogenic
929 Aeromonas hydrophila. J Fish Dis 28:437–441.

930 63. Siriyappagouder P, Shankar KM, Naveen Kumar BT, Patil R, Byadgi OV. 2014.
931 Evaluation of biofilm of Aeromonas hydrophila for oral vaccination of Channa striatus.
932 Fish Shellfish Immunol 41:581–585.

933 64. Scopes RK. 1974. Measurement of protein by spectrophotometry at 205 nm. Anal
934 Biochem 59:277–282.

65. Pang Z, Chong J, Zhou G, de Lima Morais DA, Chang L, Barrette M, Gauthier C, Jacques P-É, Li S, Xia J. 2021. MetaboAnalyst 5.0: narrowing the gap between raw spectra and functional insights. Nucleic Acids Res 49:W388–W396.

66. Goedhart J, Luijsterburg MS. 2020. VolcaNoseR is a web app for creating, exploring, labeling and sharing volcano plots. Sci Rep 10:20560.

67. Huerta-Cepas J, Szklarczyk D, Heller D, Hernández-Plaza A, Forslund SK, Cook H, Mende DR, Letunic I, Rattei T, Jensen LJ, von Mering C, Bork P. 2019. eggNOG 5.0: a hierarchical, functionally and phylogenetically annotated orthology resource based on 5090 organisms and 2502 viruses. Nucleic Acids Research 47:D309–D314.

68. Szklarczyk D, Gable AL, Nastou KC, Lyon D, Kirsch R, Pyysalo S, Doncheva NT, Legeay M, Fang T, Bork P, Jensen LJ, von Mering C. 2021. The STRING database in 2021: customizable protein–protein networks, and functional characterization of user-uploaded gene/measurement sets. Nucleic Acids Research 49:D605–D612.

69. Zhou Y, Zhou B, Pache L, Chang M, Khodabakhshi AH, Tanaseichuk O, Benner C, Chanda SK. 2019. Metascape provides a biologist-oriented resource for the analysis of systems-level datasets. Nat Commun 10:1523.

70. MacLean B, Tomazela DM, Shulman N, Chambers M, Finney GL, Frewen B, Kern R, Tabb DL, Liebler DC, MacCoss MJ. 2010. Skyline: an open source document editor for creating and analyzing targeted proteomics experiments. Bioinformatics 26:966–968.

71. Spitzer M, Wildenhain J, Rappsilber J, Tyers M. 2014. BoxPlotR: a web tool for generation of box plots. Nat Methods 11:121–122.

FIGURE LEGENDS

Figure 1| Overview of sample collection and experimental workflow: (**A)** Rohu collected from the outbreak farm was screened, kidney sample was streaked onto TSA plate; identical colonies were selected from TSA plate followed by DNA isolation, targeted Polymerase Chain Reaction (PCR) for 16sRNA gene and sequencing for identification of bacteria. To re-confirm MT374248 isolated strain, *A. hydrophila* from MTCC culture (1739T) was used. For challenge study, Phosphate Buffer saline (PBS) and *A. hydrophila* was injected intraperitoneally to Control and AH group (*Ah* challenged) respectively. After 48h of infection, fish were euthanized and liver samples were collected (Details in text). (**B)** For proteomics analysis, tissues were lysed in Sodium dodecyl sulphate (SDS) containing buffer followed by protein digestion using filter assisted sample preparation (FASP) method. Peptide samples were cleaned before subjecting to mass spectrometry for Data dependent acquisition (DDA). (**C)** Acquired raw mass spectrometry data (.raw) was analysed using MaxQuant software for identification and quantification of proteins. Statistical analysis was performed to identify the differentially expressed proteins followed by functional analysis. **(D)** Targeted proteomic validation of selected proteins using selected reaction monitoring was done where peptide sample was subjected to High performance liquid chromatography (HPLC) followed by target precursor and transition selection in Triple quadrupole mass spectrometer for acquisition of spectral data. SRM data was analysed using Skyline software where targeted data was compared with Spectral library prepared from DDA data.

Figure 2| Shotgun proteomic analysis reveals altered host proteomic signatures in liver during *Ah* infection: (A) Volcano plot depicting significantly altered protein candidates (Fold Change 1.5, $p \leq 0.05$), where red and blue colours represent upregulated and downregulated proteins respectively. (**B)** Top 30 altered key proteins found on the basis of VIP Score. **(C)** Heatmap showing differential expression (abundances) of top 30 significant proteins (Student t-test, $p \leq 0.05$) across 4 replicates of control tissues (C-1, 2, 3, 4) and 3 replicates of *Ah* infected tissues (AH-2, 3, 4). **(D)** Bar graphs representing altered abundances of six functionally important proteins (three up and three downregulated) across Control and AH group. **(E)** Pathway enrichment network (using Metascape) showing functional annotation of protein coding genes. Each gene ontology (GO) and/ or pathway term is represented by a circle node, where its size is proportional to the number of input genes mapped to that GO term, and nodes present within specific circle belong to the same cluster. Terms with a similarity score > 0.3 are linked by an edge (the thickness of the edge represents the similarity score). Color codes for pie sector represents attributes of genes from two input lists i.e., red and blue colour represent number of gene candidates mapped from list 1 (DR_Control: downregulated significant and Control enriched proteins) and list 2 (UR_AH: upregulated significant and disease enriched protein set), respectively.

Figure 3| Landscape of altered pathways and interaction networks during *Ah* pathogenesis: (A) Interaction map depicting Protein-Protein interaction between significantly downregulated proteins and their involvement in altered pathways (based on STRING analysis). Bar plots showing differential protein abundance (intensity) for a few downregulated proteins (Cyp1a, Dpyd, Chuk, Cltc and Ctsf) from different pathways, based on label-free quantification (LFQ) **(B)** PPI enrichment analysis reveals top Molecular Complex Detection (MCODE) network components i.e., mRNA metabolism and Endocytosis among significant downregulated proteins and disease enriched proteins (based on Metascape analysis). **(C)** Protein-Protein interaction for significant upregulated proteins and their respective altered pathways during infections (STRING). Bar plots showing differential protein abundance

(intensity) for a few upregulated proteins (Psma5, Atp5j, Cs, Suclg2 and Fabp (Fabp1) from different pathways, based on LFQ analysis. **(D)** PPI enrichment analysis reveals top MCODE network components i.e., Translation and Proteasome among significant upregulated proteins and disease enriched proteins (Metascape).

Figure 4| Experimental validation using targeted approach for changes in protein abundance during *Ah* infection: **(A-C)** Boxplots, peak area intensities and Peak shapes for downregulated proteins viz. Bdh1, Chuk and Ugp2, respectively and **(D)** Boxplot, peak area intensity and Peak shape for upregulated protein i.e., Atp5j in the AH condition (Ah infected group) compared to the control condition. In each figure (Left-Right), Upper panel represents the protein wise intensities based on the shotgun analysis (DDA abundance) and the targeted analysis (MRM intensity), respectively for each AH and Control condition showing similar trend in both the analyses. Lower panel shows the bar plots for peak area (with dot product (dotp) value based on match with spectral library) and spectral peak group comparison for a representative peptide of the same protein. Different colors in the bar plots and spectral peaks (in lower panel) represent different product ions of the same peptide.

Figure 5| Schematic representation of interplay between host defence and pathogen survival during *Ah* infection in *L. rohita:* (A) Once the *Ah* bacterium (A. *hydrophila*) is engulfed by the host cell through phagosome, it undergoes a series of transformations by interacting with the subcompartments of the phagocytotic pathway and finally becomes phagolysosome after fusing with lysosome. During the process, the phagosome becomes highly acidic through proton pumping by VATPase, which is essential for the intracellular killing of microbe. Material that is not useful is exported through exocytosis. In the infected host cell, several proteins involved in phagocytosis-exocytosis pathway include Rab proteins, clathrin, lysosomal-associated membrane proteins (LAMP), lysosomal integral membrane protein (Scrab2), VATPase, hydrolases and proteases (cathepsin, Tpp1). During *Ah* infection, many of the host proteins are dysregulated, and this may help bacteria survive inside the host cells. **(B)** During *Ah* infection, bacteria may escape autophagy and apoptosis of infected cell by affecting Toll like receptor (TLR3) and C-reactive lectin (CLEC4e) mediated signalling. TLR and CLEC4 identify pathogen associated molecular patterns to activate signaling cascades for inflammatory and antimicrobial effects including apoptosis. TLR3 stimulates the TRIF mediated signaling involving TRAF that finally activates MAP kinase (MEK1/2), NF-Kb or Activator protein (AP) pathways. CLEC4e works through ITAM-tyrosine kinase SYK pathway to activate signaling cascade through PLCγ2 for inducing the NFAT/ calcineurin pathway. **(C)** During *Ah* infection, host (immune) cells undergo metabolic reprogramming that may be beneficial for inflammatory host response. The increase in the rate of glycolysis in the host cell degrades glucose into pyruvate through a series of reactions. Expression of glycolysis linked enzymes (Pfk2, Eno1, Ugp2) supports glycolytic flux to form pyruvate. Pyruvate enters into the Citric acid cycle (TCA). Infection mediated metabolic reprogramming leads to functional breaks in the TCA cycle which favour the accumulation of Citrate and Succinate. Downstream metabolite of Citrate (Itaconate) inhibits SDH activity that further increases Succinate. These metabolites increase the mitochondrial reactive oxygen species (mROS) and (Nitric oxide) that have inflammatory effects. Succinate accumulation and redox-environment changes in mitochondria interfere with electron transport chain and stabilise the HIF-1α leading to the expression of MHC Class II and IL-1β. Activated HIF-1α and IL-1β further increase glycolysis and lactate production by increasing Lactate dehydrogenase activity. Fatty acid synthesis increases as a result of Citrate accumulation in cytosol and is required for energy homeostasis and inflammation that may be utilised by the bacteria. In the late infection stage, PPAR signaling gets activated and regulates the ROS mediated apoptosis and anti-inflammatory

response. (Single red down arrow- Down regulated protein, Double red down arrow- Protein enriched in controls and not detected/quantified in AH group, Single green up arrow- Upregulated protein, Double green up arrow- Protein enriched in AH group and not detected/quantified in Control group).

Figure 1

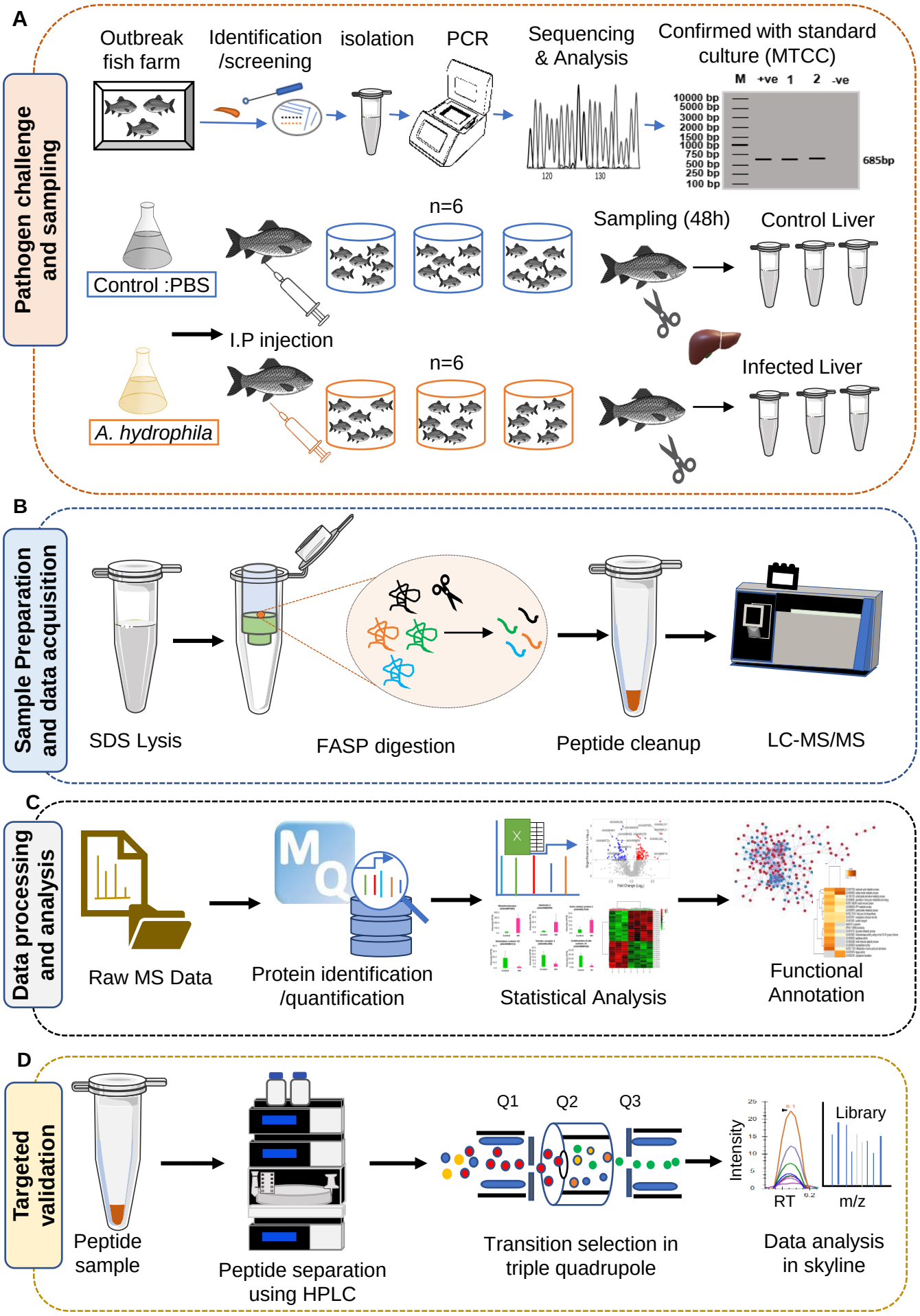
A
Pathogen challenge and sampling
Outbreak fish farm
Identification /screening
isolation
PCR
Sequencing & Analysis
Confirmed with standard culture (MTCC)
M +ve 1 2 -ve
10000 bp
5000 bp
3000 bp
2000 bp
1500 bp
1000 bp
750 bp
500 bp
250 bp
100 bp
685bp
120
130
Control :PBS
n=6
Sampling (48h)
Control Liver
I.P injection
A. hydrophila
n=6
Infected Liver
B
Sample Preparation and data acquisition
SDS Lysis
FASP digestion
Peptide cleanup
LC-MS/MS
C
Data processing and analysis
Raw MS Data
Protein identification /quantification
Statistical Analysis
Functional Annotation
D
Targeted validation
Peptide sample
Peptide separation using HPLC
Q1
Q2
Q3
Transition selection in triple quadrupole
Intensity
RT
m/z
Library
Data analysis in skyline

Figure 2

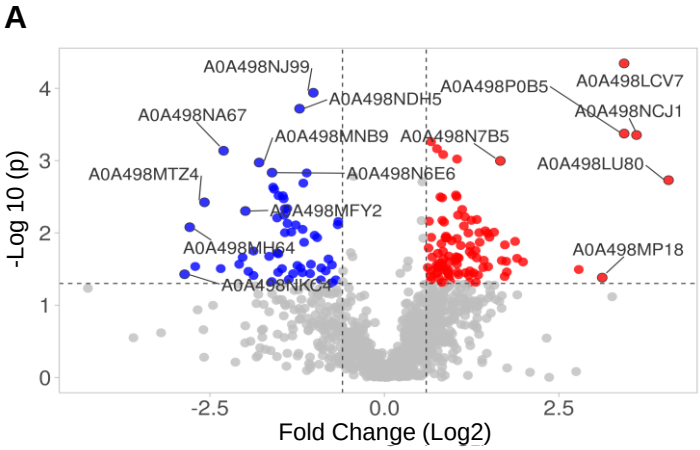
A
A0A498NJ99
A0A498NDH5
A0A498P0B5
A0A498LCV7
A0A498NA67
A0A498NCJ1
A0A498MNB9
A0A498N7B5
A0A498LU80
A0A498MTZ4
A0A498N6E6
A0A498MFY2
A0A498MH64
A0A498MP18
A0A498NKC4
-Log 10 (p)
Fold Change (Log2)

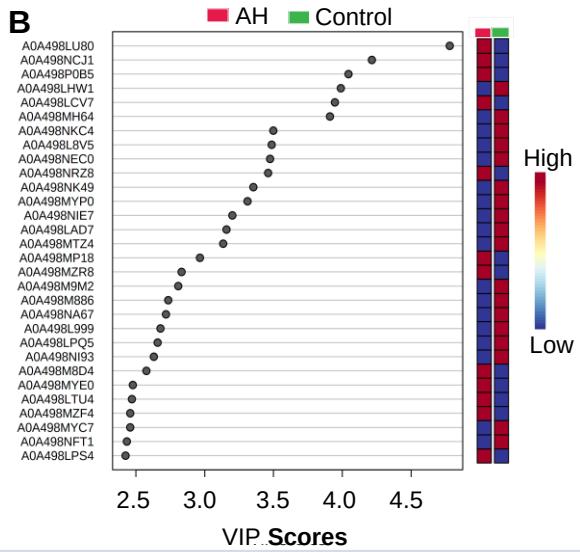
B
AH
Control
High
Low
VIP Scores

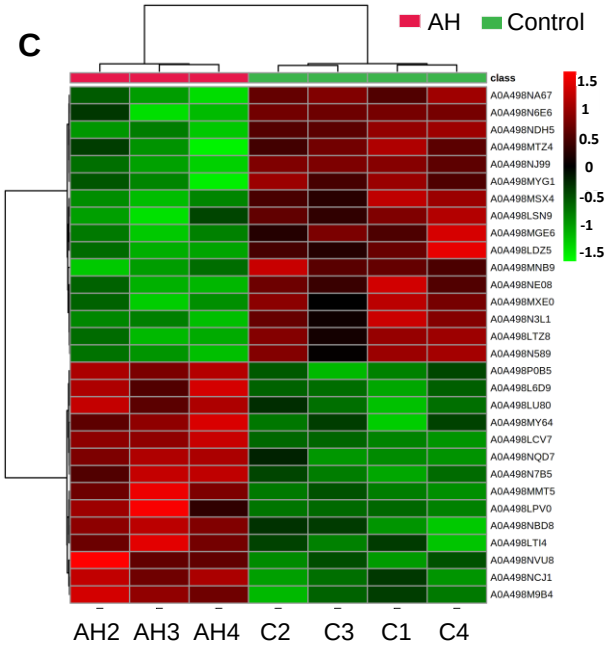
C
AH
Control
class
AH2
AH3
AH4
C2
C3
C1
C4

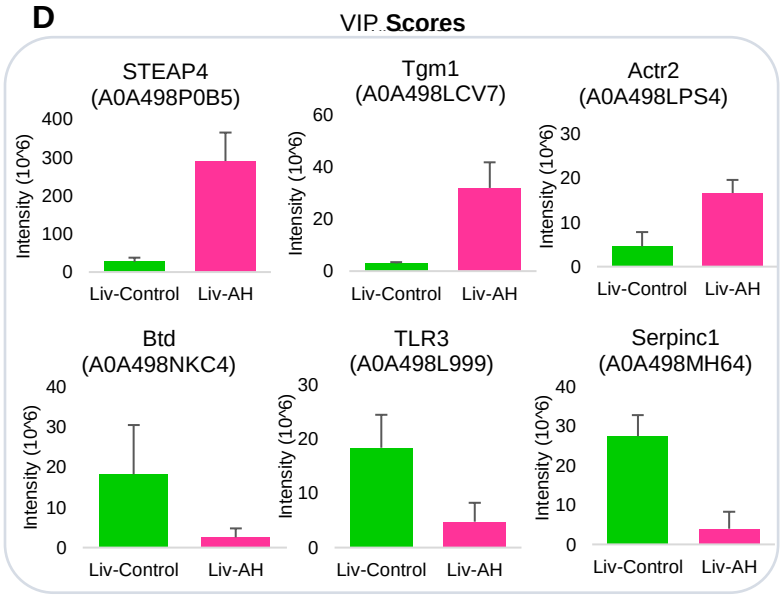
D
STEAP4 (A0A498P0B5)
Tgm1 (A0A498LCV7)
Actr2 (A0A498LPS4)
Btd (A0A498NKC4)
TLR3 (A0A498L999)
Serpinc1 (A0A498MH64)
Intensity (10^6)
Liv-Control
Liv-AH

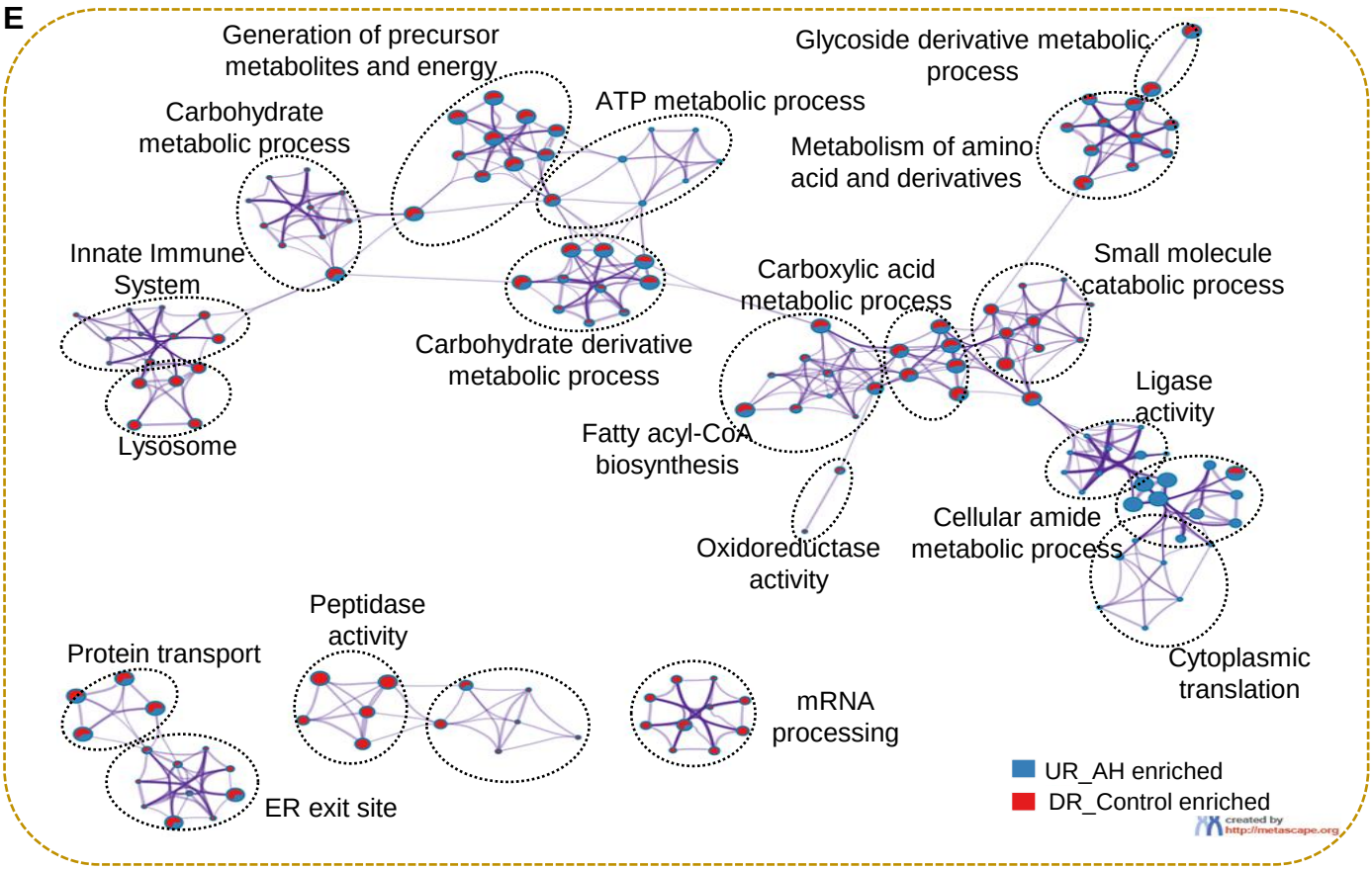
E
Generation of precursor metabolites and energy
Carbohydrate metabolic process
ATP metabolic process
Glycoside derivative metabolic process
Metabolism of amino acid and derivatives
Innate Immune System
Carbohydrate derivative metabolic process
Carboxylic acid metabolic process
Small molecule catabolic process
Lysosome
Fatty acyl-CoA biosynthesis
Ligase activity
Oxidoreductase activity
Cellular amide metabolic process
Cytoplasmic translation
Peptidase activity
Protein transport
mRNA processing
ER exit site
UR_AH enriched
DR_Control enriched
created by http://metascape.org

Figure 3

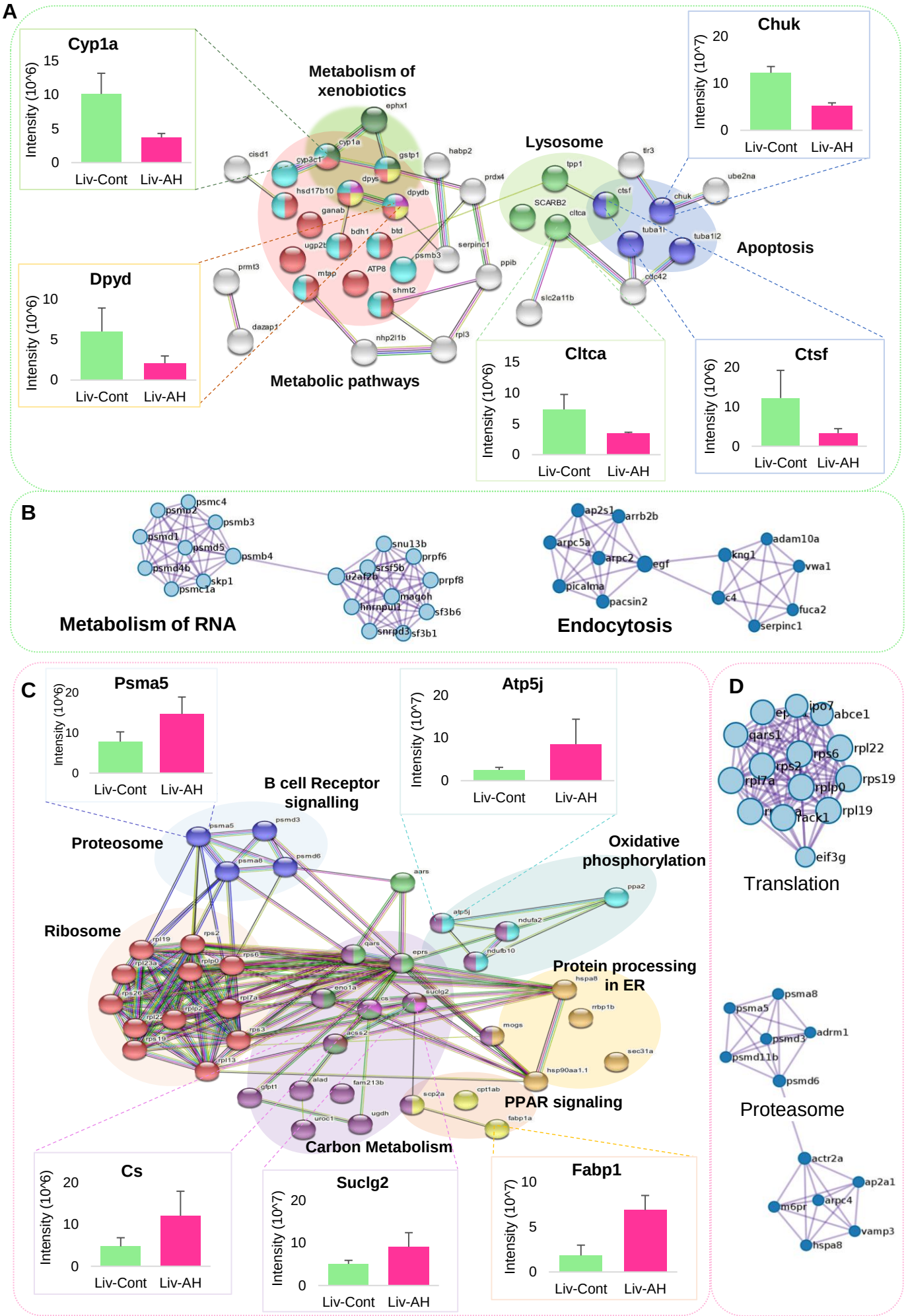
A
Cyp1a
Intensity (10^6)
15
10
5
0
Liv-Cont
Liv-AH
Metabolism of xenobiotics
ephx1
cyp1a
cisd1
cyp2c1
gstp1
habp2
prdx4
dpys
hsd17b10
dpydb
ganab
bdh1
btd
ugp2b
psmb3
serpinc1
ppib
prmt3
mtap
ATP8
shmt2
dazap1
nhp2l1b
rpl3
Metabolic pathways
Lysosome
tpp1
tlr3
ube2na
SCARB2
cltca
ctsf
chuk
tuba1l
tuba1l2
cdc42
slc2a11b
Apoptosis
Chuk
Intensity (10^7)
20
10
0
Dpyd
Cltca
Ctsf
B
psmc4
psmb2
psmb3
psmd1
psmd5
psmb4
psmd4b
skp1
psmc1a
snu13b
prpf6
srsf5b
tl2af2b
prpf8
magoh
hnrnpul1
sf3b6
snrpd3
sf3b1
Metabolism of RNA
ap2s1
arrb2b
arpc5a
arpc2
egf
picalma
pacsin2
adam10a
kng1
vwa1
c4
fuca2
serpinc1
Endocytosis
C
Psma5
Atp5j
B cell Receptor signalling
Proteosome
psma5
psmd3
psma8
psmd6
Oxidative phosphorylation
aars
ppa2
atp5j
ndufa2
ndufb10
Ribosome
rpl19
rps2
rplp0
rps6
rpl23a
qars
eprs
rps26
eno1a
rpl7a
cs
suclg2
rplp2
rpl22
rps3
acss2
rps19
rpl13
mogs
rrbp1b
sec31a
hspa8
hsp90aa1.1
Protein processing in ER
alad
gfpt1
fam213b
scp2
cpt1ab
ugdh
uroc1
fabp1a
PPAR signaling
Carbon Metabolism
Cs
Suclg2
Fabp1
D
ipo7
abce1
ep
qars1
rps6
rpl22
rps2
rpl7a
rplp0
rps19
rack1
rpl19
eif3g
Translation
psma8
psma5
adrm1
psmd3
psmd11b
psmd6
Proteasome
actr2a
ap2a1
m6pr
arpc4
vamp3
hspa8

Figure 4

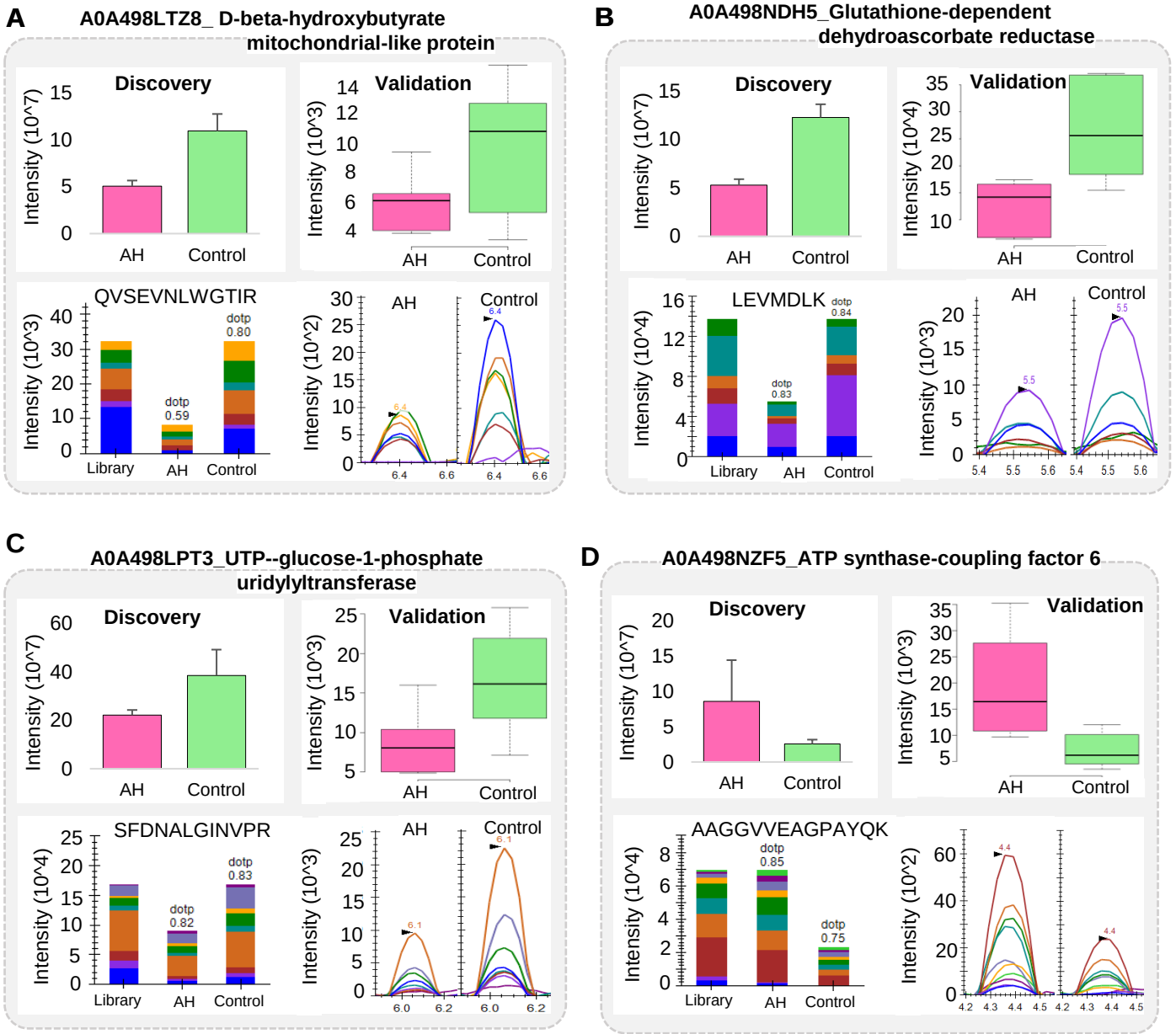
A
A0A498LTZ8_ D-beta-hydroxybutyrate mitochondrial-like protein
Discovery
Intensity (10^7)
AH
Control
Validation
Intensity (10^3)
QVSEVNLWGTIR
dotp 0.80
dotp 0.59
Library
B
A0A498NDH5_Glutathione-dependent dehydroascorbate reductase
Intensity (10^4)
LEVMDLK
dotp 0.84
dotp 0.83
C
A0A498LPT3_UTP--glucose-1-phosphate uridylyltransferase
SFDNALGINVPR
dotp 0.83
dotp 0.82
D
A0A498NZF5_ATP synthase-coupling factor 6
AAGGVVEAGPAYQK
dotp 0.85
dotp 0.75

Figure 5

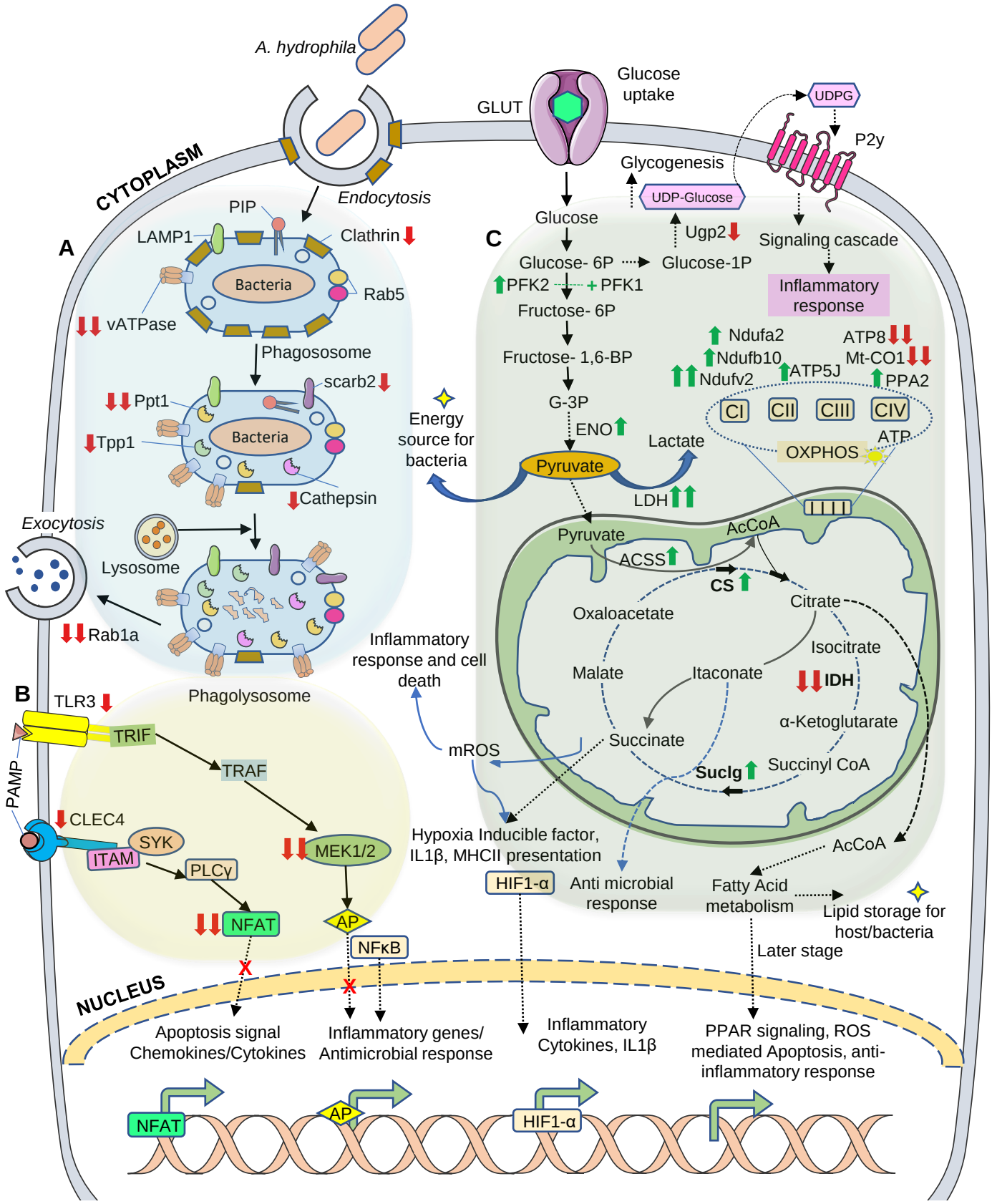
A. hydrophila
CYTOPLASM
Endocytosis
GLUT
Glucose uptake
UDPG
P2y
Glycogenesis
UDP-Glucose
Ugp2
Signaling cascade
Inflammatory response
A
PIP
LAMP1
Clathrin
Bacteria
Rab5
vATPase
Phagososome
scarb2
Ppt1
Tpp1
Cathepsin
Exocytosis
Lysosome
Rab1a
Phagolysosome
B
TLR3
TRIF
TRAF
PAMP
CLEC4
SYK
ITAM
PLCγ
MEK1/2
NFAT
AP
NFκB
C
Glucose
Glucose- 6P
Glucose-1P
PFK2
PFK1
Fructose- 6P
Fructose- 1,6-BP
G-3P
ENO
Pyruvate
Lactate
LDH
Energy source for bacteria
Ndufa2
Ndufb10
Ndufv2
ATP5J
ATP8
Mt-CO1
PPA2
CI
CII
CIII
CIV
OXPHOS
ATP
Pyruvate
AcCoA
ACSS
CS
Citrate
Oxaloacetate
Isocitrate
Malate
Itaconate
IDH
α-Ketoglutarate
Succinate
SucIg
Succinyl CoA
AcCoA
Inflammatory response and cell death
mROS
Hypoxia Inducible factor, IL1β, MHCII presentation
HIF1-α
Anti microbial response
Fatty Acid metabolism
Lipid storage for host/bacteria
Later stage
NUCLEUS
Apoptosis signal Chemokines/Cytokines
Inflammatory genes/ Antimicrobial response
Inflammatory Cytokines, IL1β
PPAR signaling, ROS mediated Apoptosis, anti-inflammatory response
NFAT
AP
HIF1-α